Computers and Mathematics with Applications 108 (2022) 49–65

Contents lists available at ScienceDirect

Computers and Mathematics with Applications

www.elsevier.com/locate/camwa

Angle dependence in coupling conditions for shallow water equations at channel junctions

M. Briani [a,*], G. Puppo [b], M. Ribot [c]

[a] Istituto per le Applicazioni del Calcolo "Mauro Picone", CNR, Rome, Italy
[b] Sapienza Università di Roma, Rome, Italy
[c] Institut Denis Poisson,Université d'Orléans, CNRS, France

ARTICLE INFO

Keywords:
Shallow water equations
Angle dependence in coupling conditions
Canals network
Riemann problem

ABSTRACT

In this paper we propose a modeling setting and a numerical Riemann problem solver at the junction of one dimensional shallow-water channel networks. The junction conditions take into account the angles with which the channels intersect and include the possibility of channels with different sections. The solver is illustrated with several numerical tests which underline the importance of the angle dependence to obtain reliable solutions.

1. Introduction

The shallow water model gives an approximate description of free surface water flows and takes the form of a non-linear hyperbolic system of PDE's composed of mass and momentum balance equations. It is widely used to describe flows in artificial canals and water channels with applications for instance to environmental problems. In water management issues, these equations are considered as a fundamental tool to reproduce the dynamics of networks of channels or of the branching of rivers, which may occur in different types of configurations.

The most straightforward treatment from modeling and numerical point of views consists in considering the network as a two dimensional domain covered with an unstructured grid [11,12]. However, from a computational point of view it is much more efficient to consider the network as a set of one dimensional channels coupled through junctions. The main difficulty in the construction of the model is the definition of the coupling conditions at the junction between the adjoining channels and we mention the following reviews for one-dimensional flows on networks [5,14]. The coupling condition can be seen as a Riemann problem involving a constant state for each of the adjoining channels and Riemann problems at a junction are widely discussed in literature, see [15,9,20,32,30]. To close the problem, one completes the Riemann problem with physical conservation properties across the junction, see [28,27]. The method studied in [1] consists in solving a one-dimensional flow in each channel, coupled with a 2D solution locally at the junction. This has the advantage of taking into account naturally the geometry of the junction, and it does not require a restriction to the fluvial regime. In our case, we propose coupling conditions with which one can solve the system in a purely 1D setting. In this way, our contribution is not just a numerical solver, but it is a junction model in its own right.

From a numerical point of view, one has to couple one dimensional numerical solvers in the 1D channels with an approximate junction Riemann solver, see [1,4,7,25,33].

We consider a junction of three channels and we assume by convention to have one incoming channel which ends at the junction and two outgoing channels which start at the junction. To solve the junction problem we need to find the three states (mass and discharge) corresponding to each of the three one dimensional channels at the junction for a total of six unknowns. One imposes mass conservation at the junction which yields one equation, then one formulates a left-half Riemann problem for the incoming channel and a right-half Riemann problem for each of the two outgoing channels. Under subcritical flow assumptions, we obtain therefore three more conditions. Thus, two remaining equations have to be specified in order to define the junction model. In some works the set of equations is completed by assuming the continuity of water levels [9,20,32,6] or the continuity of energy [28,25]. However, none of these works use a condition that takes into account the geometry and especially the angles formed by the channels in the fork. For various attempts to include an angle dependency in the solver, see [8,26,17]. Different approaches cover the junction with two-dimensional elements and project the computed 2D solution along the one dimensional channels [1].

* Corresponding author.
E-mail addresses: m.briani@iac.cnr.it (M. Briani), gabriella.puppo@uniroma1.it (G. Puppo), magali.ribot@univ-orleans.fr (M. Ribot).

https://doi.org/10.1016/j.camwa.2021.12.021
Received 27 March 2021; Received in revised form 8 December 2021; Accepted 28 December 2021

These studies have several applications, such as optimization [30, 23,21,22]; see also [3] for an interesting application to the modeling of a particular wave energy converter, the so-called oscillating water column.

In this article, we propose new coupling conditions at the junction that depend on the angles with which the channels intersect, allowing also for channels with different sections, [2,13,29]. Away from the junction we assume the solution to be 1D, while we describe the junction as a pointwise region where coupling occurs between the branches. We then consider the physical configuration as a 2D triangle formed by the intersection points of the walls of the three channels and, to this two dimensional domain, we apply conservation of mass and of the two components of momentum. Thanks to this procedure, we obtain for the six unknowns at the junction three 1D non linear equations which include a dependence on the angles, to be coupled with the three equations of the characteristic curves. Extending this study to a network of channels with several nodes is straightforward. This work therefore extends the results of [8] by considering branches with different sections. We also prove that our approach is a generalization of the junction conditions proposed in [28,25]. In those works, the continuity of the energy is used to provide two equations at the junction. Here, we also obtain energy continuity, but only for a particular geometrical configuration of the junction We also prove the existence of the solution of our junction Riemann problem in a few particular cases.

Validation of numerical schemes obtained in this way is carried out comparing the numerical 1D solution with the junction, with a fully 2D solver, see [17,19,24,18]. We compare therefore our numerical solver with a fully 2D solver for shallow water equations showing that the numerical approximation improves as the width of the 2D channels is reduced.

The paper is organized as follows. In Section 2, we concentrate on the solution of the Riemann problem for shallow-water equations. We then present the junction geometry in Section 3, defining our coupling conditions in Section 3.1. We discuss extensions for special configurations in Section 3.2, including also the case of a single channel with varying cross-section. In Section 4 we merge the relations at the junction with the numerical approximation of shallow water equations along the channels. Section 4.3 is devoted to a discussion of the existence of the numerical solution in a few cases. We end in Section 5 with the numerical tests.

2. The shallow water equations and its standard Riemann problem

Let us first recall the shallow water or Saint Venant equations, and some of theirs properties that will be useful in the following.

2.1. The shallow water equations

The 1D shallow water equations, introduced by Saint-Venant in [10] and derived in [16] from Navier-Stokes incompressible equations with a free moving boundary, describe the water propagation in a channel with rectangular cross-section and constant slope as follows:

$$\begin{cases} \partial_t h + \partial_x(hv) = 0, \\ \partial_t(hv) + \partial_x(hv^2 + \frac{1}{2}gh^2) = gh\partial_x(S_0 - S_f), \end{cases} \tag{1}$$

with $h(x,t)$ the water height, $v(x,t)$ the water velocity at time t and location x along the channel, g the gravity constant, S_0 the bed slope function and S_f the friction slope function. The first equation comes from mass conservation and the second one from momentum balance. For the purpose of this work, we assume a steady state friction on all channels and we assume horizontal channels with zero slope. Thus, the source term is zero.

We set $q = hv$ (the quantity hv is often called the *discharge* in shallow water theory, since it measures the flow rate of water past a point) and we reformulate system (1) in vector form as

$$\partial_t U + \partial_x f(U) = 0, \tag{2}$$

where

$$U = \begin{pmatrix} h \\ q \end{pmatrix}, \quad f(U) = \begin{pmatrix} hv \\ hv^2 + \frac{1}{2}gh^2 \end{pmatrix}. \tag{3}$$

For smooth solutions, system (2) can equivalently be written in the quasilinear form

$$\partial_t U + A(U)\partial_x U = 0, \tag{4}$$

where the Jacobian matrix $A(U) = f'(U)$ is

$$A(U) = \begin{pmatrix} 0 & 1 \\ -v^2 + gh & 2v \end{pmatrix}, \tag{5}$$

with eigenvalues

$$\lambda_1(U) = v - \sqrt{gh}, \quad \lambda_2(U) = v + \sqrt{gh}. \tag{6}$$

Note that in general $\lambda_1(U)$ and $\lambda_2(U)$ can be of either sign. When the velocity $v = q/h$ of the fluid is smaller than the speed $\sqrt{gh}$ of the gravity waves, that is $|v| < \sqrt{gh}$, the flow is said to be *fluvial* or *subcritical* and then one has

$$\lambda_1(U) < 0, \quad \lambda_2(U) > 0. \tag{7}$$

Hence, under the subcritical condition (7), there are two waves propagating in opposite directions. The left and right characteristics are associated to $\lambda_1(U)$ and $\lambda_2(U)$ respectively. The ratio $Fr = |v|/\sqrt{gh}$ is called the *Froude number* and the flow is subcritical iff $Fr < 1$.

In the following, we will assume that the initial data satisfy the *fluvial regime* condition and that the flow remains fluvial throughout time. However, other papers, see [1] for example, propose a solution of shallow water equations on networks which can be applied also in the transcritical and supercritical regimes, by considering a single 2D local element at the junction.

2.2. The standard Riemann problem for shallow-water equations

Here we are in particular interested in the solution of the Riemann problem:

$$\begin{cases} \partial_t U + \partial_x f(U) = 0, \\ U(x,0) = \begin{cases} U_l & \text{if } x < 0, \\ U_r & \text{if } x > 0, \end{cases} \end{cases} \tag{8}$$

where $U(x,0) = (h(x,0), q(x,0))^T$ is the initial condition and $U_l = (h_l, q_l)^T$ (resp. $U_r = (h_r, q_r)^T$) is the initial constant state to the left (resp. to the right) of the interface $x = 0$. The characteristic fields of the shallow water equations are genuinely nonlinear and therefore the Riemann problem always consists of two waves, each of which is either a shock or a rarefaction. Under the *subcritical flow condition* (7), there will be one left (with negative speed) and one right (with positive speed) going wave. In the sequel the left and right going waves are denoted by l-wave and r-wave, respectively. The solution of this Riemann problem consists of the l-wave and the r-wave separated by an intermediate state $\hat{U} = (\hat{h}, \hat{q})^T$. We remark that the solution at the interface $x = 0$ coincides with $\hat{U}$, which is the intersection point of the two functions W_l and W_r defined by

$$W_l(h; U_l) = \begin{cases} v_l - 2(\sqrt{gh} - \sqrt{gh_l}) & \text{if } h < h_l \text{ (rarefaction)} \\ v_l - (h - h_l)\sqrt{g\frac{h+h_l}{2hh_l}} & \text{if } h > h_l \text{ (shock wave)}, \end{cases} \tag{9}$$

and

$$W_r(h; U_r) = \begin{cases} v_r + 2(\sqrt{gh} - \sqrt{gh_r}) & \text{if } h < h_r \text{ (rarefaction)} \\ v_r + (h - h_r)\sqrt{g\frac{h+h_r}{2hh_r}} & \text{if } h > h_r \text{ (shock wave)}, \end{cases} \tag{10}$$

which return the physically correct $\hat{h}$ and $\hat{v}$ intermediate values connecting the left and right states with an entropic solution.

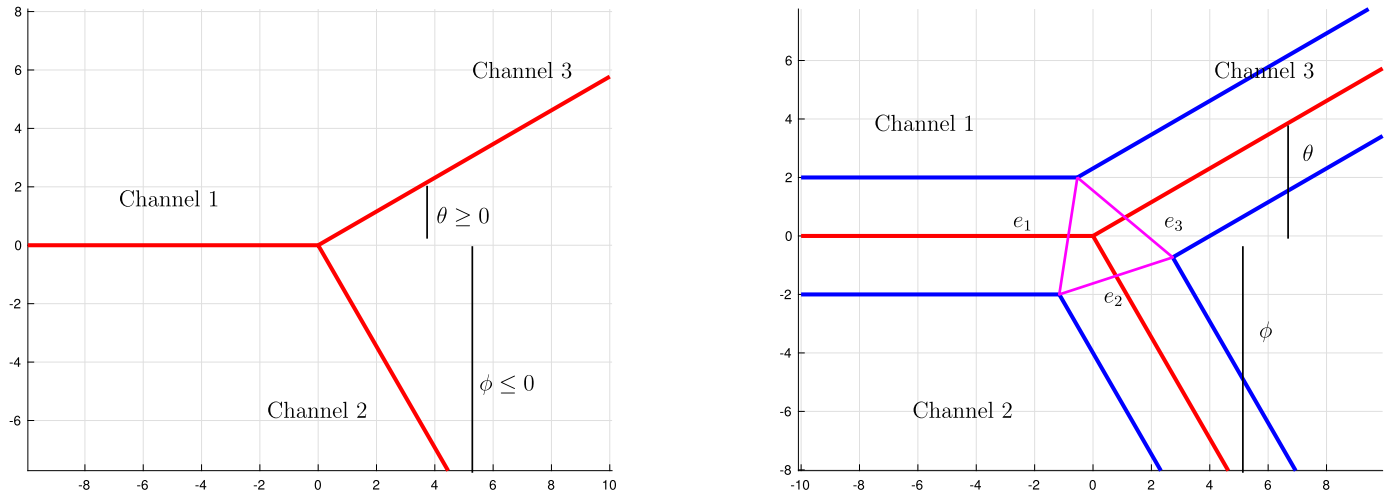

(a) 1D set-up (b) 2D configuration

Fig. 1. A 3 channel junction.

3. Angle dependent conditions at the junction

In this work, a junction is defined as the intersection of three channels. For more general cases of $N > 3$ channels, see the conclusion section.

We assume that 1D shallow water equations hold on each channel of the network and we aim at deriving coupling conditions at the junction to complete the model. These conditions enable to compute the intermediate states at the junction for the Riemann problem under consideration.

3.1. Definition of the coupling conditions at the junction

The channels will be labeled 1, 2 and 3 respectively, where channel 1 is assumed to be parallel to the x axis. We fix the origin of the reference system in the point where the three channels intersect. Let θ and ϕ be the angles that channel 3 and 2 respectively form with the x axis. We will assume that $\theta \geq 0$, while $\phi \leq 0$, obtaining the geometry in Fig. 1a. This is the one dimensional set up.

Further, we will suppose that the channels can have different widths. This case has already been considered through Riemann problems for augmented shallow water equations, allowing to consider discontinuous channel sections, see [2] for example. Let then $s_j, j = 1,2,3$ be the half-width of each channel. Therefore, we can think that the 1D setup is the core of a two dimensional junction, as shown in Fig. 1b.

Let e_k, $k = 1,2,3$, be the interface separating the k-th channel from the junction, that is to say the edge of the internal triangle common with channel k, see Fig. 1b. Let U_k^*, $k = 1,2,3$, denote the state variable in channel k at the side of e_k obtained with the 1D solver used in the channel, while U_k, $k = 1,2,3$, is the state variable at the side of e_k inside the junction. The purpose of the junction Riemann solver is to compute U_k given U_k^*. Since each state consists of the couple (h, v), we need to find 6 unknowns at the junction. Thanks to the fluvial regime hypothesis, three conditions are obtained finding the intermediate states of the one dimensional Riemann problem defined at each interface e_k and in order to compute the three other missing data we shift to the 2D setting of Fig. 1b. We consider the triangle formed by the intersection points of the walls of the three channels, and to this two dimensional domain we apply conservation of mass and of the two components of momentum, which gives us the 3 missing equations. Once the three states U_k, $k = 1,2,3$, at the junction have been computed, we have at each interface e_k the left and right states which are needed to compute the numerical flux at the boundary interfaces of the channels.

Note that other forms of control volumes can be considered. However, we focus here on triangles, which are entirely internal to the channels, avoiding therefore to impose arbitrary conditions on the external boundaries.

3.1.1. Junction conditions derived from the Riemann solver

Let us begin with the 3 equations derived from the Riemann solver. We emphasize that, by convention, the given configuration fixes channel 1 as entering the junction and channels 2 and 3 as leaving the junction.

Three relations are obtained matching the unknowns U_k at the junction with the data U_k^* coming from the three channels through equations (9) and (10). More precisely,

$$\begin{aligned} v_1 &= W_l(h_1; U_1^*) \\ v_2 &= W_r(h_2; U_2^*) \\ v_3 &= W_r(h_3; U_3^*). \end{aligned} \tag{11}$$

We note again that this construction requires a *fluvial regime*, in which only one wave exits the junction towards each of the three adjoining channels. As far as we know, it is not possible to determine conditions on data U_k^* that ensure that the flow remains in the fluvial regime.

3.1.2. Junction conditions coming from mass and momentum conservation

We now derive the 3 supplementary equations coming from conservation of mass and of the two components of momentum. For that purpose, we come back to the 2D configuration of the junction and we use the following notation

- h denotes the height of water in the 2D configuration,
- $\mathbf{v} = (v_x, v_y)^T$, denotes the 2D velocity in the 2D junction domain,
- $\mathbf{q} = h\mathbf{v} = h(v_x, v_y)^T$ denotes the 2D discharge,
- h_k and $\mathbf{q}_k = h_k(v_{x,k}, v_{y,k})^T$, $k = 1,2,3$, denote the average height and the average discharge over the edge e_k of the junction triangle corresponding to channel k, see Fig. 1b.

We first recall the shallow-water equations in 2D, composed of the mass conservation equation and of the momentum conservation equation:

$$\begin{cases} \partial_t h + \nabla \cdot (h\mathbf{v}) = 0, \\ \partial_t (h\mathbf{v}) + \nabla \cdot (h\mathbf{v} \otimes \mathbf{v}) + \nabla(\frac{1}{2} g h^2) = 0. \end{cases} \tag{12}$$

In the following, we call T the triangle formed by the intersection points of the walls of the three channels and its boundary ∂T is composed of three edges e_k, $k = 1,2,3$, see Fig. 1b.

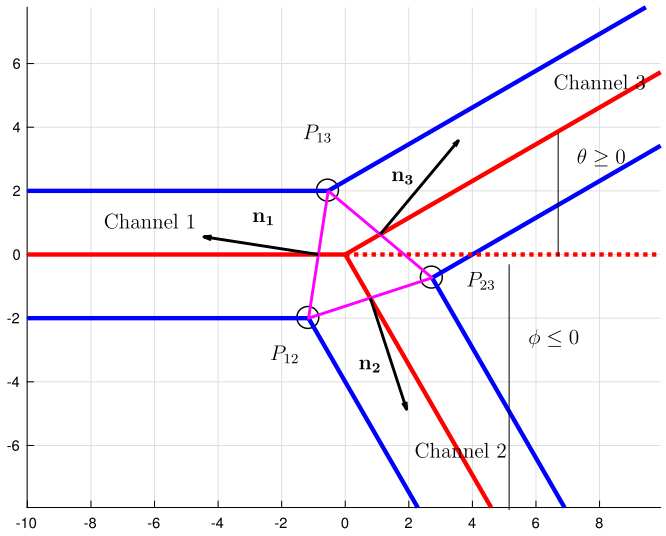

Fig. 2. A 3 channel junction. Illustration of the geometrical notation. Parameters are $s_1 = s_2 = s_3 = 2$, $\theta = \frac{\pi}{6}$ and $\phi = -\frac{\pi}{3}$.

We assume that mass and momentum are conserved in triangle T, that is to say $\int_T h(t,x)dx$ and $\int_T h\mathbf{v}(t,x)dx$ are preserved at all times. Integrating Eq. (12) on the triangle T yields therefore for the mass conservation

$$\int_{\partial T} \mathbf{q}\cdot\mathbf{n} = 0, \text{ with } \mathbf{q} = h\mathbf{v}, \tag{13}$$

where $\mathbf{n}$ is the outer normal of ∂T, while the conservation of the two components of momentum gives the two relations

$$\int_{\partial T} \left(v_x \mathbf{q} + \frac{1}{2} g h^2 \begin{pmatrix} 1 \\ 0 \end{pmatrix} \right) \cdot \mathbf{n} = 0, \tag{14}$$

and

$$\int_{\partial T} \left(v_y \mathbf{q} + \frac{1}{2} g h^2 \begin{pmatrix} 0 \\ 1 \end{pmatrix} \right) \cdot \mathbf{n} = 0. \tag{15}$$

Decomposing ∂T as the sum of the three edges e_k, $k = 1,2,3$, the three conditions at the junction, given by mass conservation and the two components of momentum conservation, can then be written as:

$$\sum_{k=1,2,3} \ell_k \mathbf{q}_k \cdot \mathbf{n}_k = 0, \tag{16a}$$

$$\sum_{k=1,2,3} \ell_k \left(v_{x,k} \mathbf{q}_k + \frac{1}{2} g h_k^2 \begin{pmatrix} 1 \\ 0 \end{pmatrix} \right) \cdot \mathbf{n}_k = 0, \tag{16b}$$

$$\sum_{k=1,2,3} \ell_k \left(v_{y,k} \mathbf{q}_k + \frac{1}{2} g h_k^2 \begin{pmatrix} 0 \\ 1 \end{pmatrix} \right) \cdot \mathbf{n}_k = 0, \tag{16c}$$

where ℓ_k is the length of the edge e_k of the triangle, $\mathbf{n}_k$ is the outer normal to e_k and $\mathbf{q}_k$ is the average of $\mathbf{q}$ on the side e_k of the triangle.

To specify all quantities appearing in system (16), we need to compute the normals $\mathbf{n}_k$ to the sides of the triangle and their lengths ℓ_k. To fix notation, refer to Fig. 2.

To begin with, we need to give the coordinates of the intersection points of the walls, namely points P_{12}, P_{13} and P_{23} that are displayed on Fig. 2. Let us recall that θ and ϕ are the angles of channels 2 and 3 with the x-axis, while $2s_k$ is the section of channel k.

The equations for the straight lines composing the 1D skeleton of Fig. 1a written in parametric form are

$$y_1 = t_1(1,0)^T,$$
$$y_2 = t_2(\cos\phi, \sin\phi)^T,$$
$$y_3 = t_3(\cos\theta, \sin\theta)^T,$$

with $t_k \in \mathbb{R}, k = 1,2,3$. Then, to obtain the walls of the channels, i.e., to construct the 2D setting of Fig. 2, we just need to write the equations of the two straight lines parallel to the axis y_k at the center of the channel, and at a distance $\pm s_k$ from the axis, for each channel. The walls of the three channels are

$$\begin{aligned} y_1^{\pm} &= t_1(1,0)^T \pm s_1(0,1)^T, \\ y_2^{\pm} &= t_2(\cos\phi, \sin\phi)^T \pm s_2(-\sin\phi, \cos\phi)^T, \\ y_3^{\pm} &= t_3(\cos\theta, \sin\theta)^T \pm s_3(-\sin\theta, \cos\theta)^T. \end{aligned} \tag{17}$$

The triangle in Fig. 2 across which the 2D interaction occurs is obtained intersecting the straight lines defining the walls of the channels. More precisely, P_{13}, is the intersection of y_1^+ with y_3^+, P_{12} is defined by the intersection of y_1^- with y_2^-, and the last point P_{23} lies at the intersection of y_3^- and y_2^+. We obtain,

$$P_{13}\left(\frac{s_1\cos\theta - s_3}{\sin\theta}, s_1 \right), \quad \theta \neq 0. \tag{18}$$

If $\theta = 0$, the system has a solution only provided $s_1 = s_3$, and the two straight lines actually coincide. In this case we define $P_{13} = (0, s_1)$.

Analogously,

$$P_{12}\left(\frac{-s_1\cos\phi + s_2}{\sin\phi}, -s_1 \right), \quad \phi \neq 0. \tag{19}$$

If $\phi = 0$, we must have $s_1 = s_2$, and we pick $P_{12} = (0, -s_1)$. With this approach, we cannot treat the case in which both $\phi = \theta = 0$, unless we consider the two channels y_2 and y_3 superposed one on top of the other. We will see in the next subsection how to extend the construction also to the case $\phi = \theta = 0$.

Finally,

$$P_{23}\left(\frac{s_3\cos\phi + s_2\cos\theta}{\sin(\theta-\phi)}, \frac{s_3\sin\phi + s_2\sin\theta}{\sin(\theta-\phi)} \right). \tag{20}$$

The quantity $\sin(\phi - \theta)$ can be zero either for $\phi = \theta = 0$, in which case the two channels coincide, or when $\phi = -\pi/2$ and $\theta = \pi/2$. In that case, a solution exists only for $s_3 = s_2$, which means that y_3^- and y_2^+ coincide, and we fix the intersection point to $P_{23} = (s_3, 0)$.

We will analyze, and extend, the particular cases $\theta = 0, \phi = 0, (\theta, \phi) = (\pi/2, -\pi/2)$ in the following section.

Once the points P_{13}, P_{12}, P_{23} are defined, we can compute all quantities $\mathbf{n}_1$, $\mathbf{n}_2$, $\mathbf{n}_3$, ℓ_1, ℓ_2 and ℓ_3 depending on the geometry appearing in (16). The length of the sides is

$$\ell_1 = ||P_{13} - P_{12}||, \qquad \ell_2 = ||P_{23} - P_{12}||, \qquad \ell_3 = ||P_{23} - P_{13}||, \tag{21}$$

and the normals are

$$\mathbf{n}_1 = \frac{1}{\ell_1} \begin{pmatrix} -2s_1 \\ \dfrac{s_1\sin(\theta+\phi) - s_2\sin\theta - s_3\sin\phi}{\sin\phi\sin\theta} \end{pmatrix},$$

$$\mathbf{n}_2 = \frac{1}{\ell_2} \begin{pmatrix} s_1 + \dfrac{s_2\sin\theta + s_3\sin\phi}{\sin(\theta-\phi)} \\ -\dfrac{s_2\cos\theta + s_3\cos\phi}{\sin(\theta-\phi)} - \dfrac{s_1\cos\phi - s_2}{\sin\phi} \end{pmatrix},$$

$$\mathbf{n}_3 = \frac{1}{\ell_3} \begin{pmatrix} s_1 - \dfrac{s_2\sin\theta + s_3\sin\phi}{\sin(\theta-\phi)} \\ \dfrac{s_2\cos\theta + s_3\cos\phi}{\sin(\theta-\phi)} - \dfrac{s_1\cos\theta - s_3}{\sin\theta} \end{pmatrix}.$$

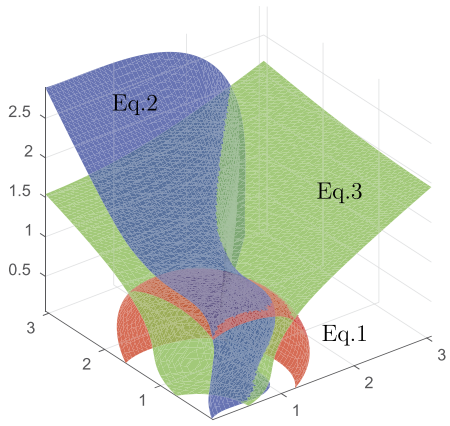

(a) Zero surfaces of the three equations in (24).

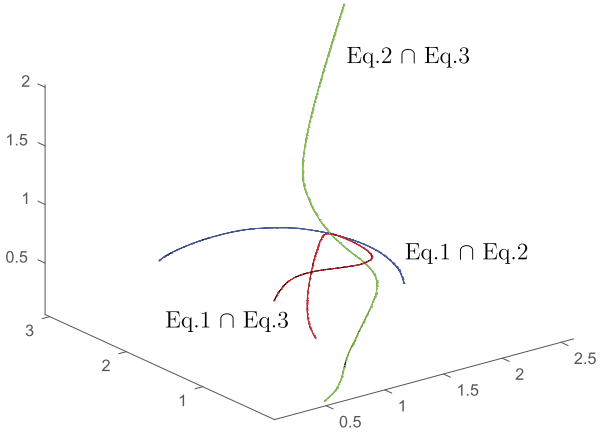

(b) Intersection point of the three zero surfaces.

Fig. 3. Graphic illustration of the existence of a unique solution of system (11)-(24) for the parameters $s_1 = s_2 = s_3 = 1$, $\theta = -\phi = \pi/6$ and $U_1^* = (1.5, 0)^T$, $U_2^* = U_3^* = (1, 0)^T$.

Remark 1. The construction is well defined as long as the triangle formed by P_{13}, P_{12}, P_{23} is non degenerate. We say that the triangle is degenerate when the three points lie on the same straight line. Straightforward computations show that this occurs when $\det(\mathbf{n}_1, \mathbf{n}_3) = 0$ which is equivalent to the particular combination

$$(s_1 \sin(\theta - \phi) + s_3 \sin(\phi) - s_2 \sin(\theta))^2 + 4 s_2 s_3 \sin(\phi) \sin(\theta) = 0. \tag{22}$$

In the frame of reference we have chosen, the discharge in the three channels can be written as

$$\mathbf{q}_1 = q_1 \begin{pmatrix} 1 \\ 0 \end{pmatrix}, \quad \mathbf{q}_2 = q_2 \begin{pmatrix} \cos\phi \\ \sin\phi \end{pmatrix}, \quad \mathbf{q}_3 = q_3 \begin{pmatrix} \cos\theta \\ \sin\theta \end{pmatrix}, \tag{23}$$

where $q_k = \|\mathbf{q}_k\|$.

Let $v_k = q_k / h_k$ be the velocity along the k-th channel. Then the conservation laws (16) across the junction can be written as

$$\ell_1 h_1 v_1 \begin{pmatrix} 1 \\ 0 \end{pmatrix} \cdot \mathbf{n}_1 + \ell_2 h_2 v_2 \begin{pmatrix} \cos\phi \\ \sin\phi \end{pmatrix} \cdot \mathbf{n}_2 + \ell_3 h_3 v_3 \begin{pmatrix} \cos\theta \\ \sin\theta \end{pmatrix} \cdot \mathbf{n}_3 = 0, \tag{24a}$$

$$\begin{aligned} &\ell_1 \left(h_1 v_1^2 \begin{pmatrix} 1 \\ 0 \end{pmatrix} + \frac{1}{2} g h_1^2 \begin{pmatrix} 1 \\ 0 \end{pmatrix} \right) \cdot \mathbf{n}_1 \\ &+ \ell_2 \left(h_2 v_2^2 \cos\phi \begin{pmatrix} \cos\phi \\ \sin\phi \end{pmatrix} + \frac{1}{2} g h_2^2 \begin{pmatrix} 1 \\ 0 \end{pmatrix} \right) \cdot \mathbf{n}_2, \\ &+ \ell_3 \left(h_3 v_3^2 \cos\theta \begin{pmatrix} \cos\theta \\ \sin\theta \end{pmatrix} + \frac{1}{2} g h_3^2 \begin{pmatrix} 1 \\ 0 \end{pmatrix} \right) \cdot \mathbf{n}_3 = 0, \end{aligned} \tag{24b}$$

$$\begin{aligned} &\ell_1 \left(\frac{1}{2} g h_1^2 \begin{pmatrix} 0 \\ 1 \end{pmatrix} \right) \cdot \mathbf{n}_1 + \ell_2 \left(h_2 v_2^2 \sin\phi \begin{pmatrix} \cos\phi \\ \sin\phi \end{pmatrix} + \frac{1}{2} g h_2^2 \begin{pmatrix} 0 \\ 1 \end{pmatrix} \right) \cdot \mathbf{n}_2 \\ &+ \ell_3 \left(h_3 v_3^2 \sin\theta \begin{pmatrix} \cos\theta \\ \sin\theta \end{pmatrix} + \frac{1}{2} g h_3^2 \begin{pmatrix} 0 \\ 1 \end{pmatrix} \right) \cdot \mathbf{n}_3 = 0, \end{aligned} \tag{24c}$$

where we used the fact that the axis of channel 1 is parallel to the x axis.

3.1.3. Solutions for the whole system of equations at the junction

Combining the three equations (24) with the three equations (11) coupling the states in the junction with the 1D channels, we find a system of 6 non linear equations at the junction, whose solution is given by the three intermediate states $U_k = (h_k, v_k)^T$, $k = 1, 2, 3$.

Remark 2. If we consider a stationary solution of (1) such that the velocity is null and the height is constant in space, i.e. $h_k^* = \bar{h}$ and $v_k^* = 0$, $k = 1, 2, 3$ then $h_k = \bar{h}$ and $v_k = 0$ $k = 1, 2, 3$ is a trivial solution of system (24)-(11) since $\mathbf{n}_1 + \mathbf{n}_2 + \mathbf{n}_3 = 0$. This means that the coupling condition at the junction preserves the lake at rest stationary solution on the whole network.

Substituting v_1, v_2, v_3 from (11) into (24), we find a system of three non linear equations in the three unknowns h_1, h_2 and h_3 which gives the solution at the junction. Once the parameters s_1, s_2, s_3, θ, ϕ and U_1^*, U_2^*, U_3^* are fixed, these three equations define three hypersurfaces whose zeros surfaces can be plotted in h_1, h_2 and h_3 coordinates, see Fig. 3a. The intersection of these surfaces is the required solution and an example is shown in Fig. 3b.

3.2. Special cases and extensions

In this section, we consider three particular cases.

We start with the simplified case in which the channels are orthogonal to the sides of the triangle. In that case, the junction is defined uniquely by the three sections and the equations (24) simplify loosing the dependency on the angles. In this case, see Fig. 4, it is easy to see that the angles θ and ϕ defining the skeleton of the junction coincide with the angles labeled θ and ϕ internal to the triangle in Fig. 4, and the length of the sides coincides with the width of the channels, namely $l_k = 2 s_k$, $k = 1, 2, 3$.

Then, it is straightforward to see that the sections depend on the angles through the following relations

$$\begin{aligned} &s_2 \sin\phi + s_3 \sin\theta = 0, \\ &s_1 = s_2 \cos\phi + s_3 \cos\theta. \end{aligned} \tag{25}$$

Since in the present case, $\mathbf{q}_k$ is parallel to $\mathbf{n}_k$, equation (16a) becomes

$$-s_1 q_1 + s_2 q_2 + s_3 q_3 = 0. \tag{26}$$

Equation (16b)-(16c), corresponding to the conservation of momentum at the junction in 2D give:

$$\left(\frac{q_1^2}{h_1} + \frac{1}{2} g h_1^2 \right) s_1 = \left(\frac{q_2^2}{h_2} + \frac{1}{2} g h_2^2 \right) s_2 \cos\phi + \left(\frac{q_3^2}{h_3} + \frac{1}{2} g h_3^2 \right) s_3 \cos\theta \tag{27}$$

and

$$0 = \left(\frac{q_2^2}{h_2} + \frac{1}{2} g h_2^2 \right) s_2 \sin\phi + \left(\frac{q_3^2}{h_3} + \frac{1}{2} g h_3^2 \right) s_3 \sin\theta. \tag{28}$$

Using the identities in (25), we can rewrite (27) and (28) as

$$\frac{q_1^2}{h_1} + \frac{1}{2} g h_1^2 = \frac{q_2^2}{h_2} + \frac{1}{2} g h_2^2 = \frac{q_3^2}{h_3} + \frac{1}{2} g h_3^2.$$

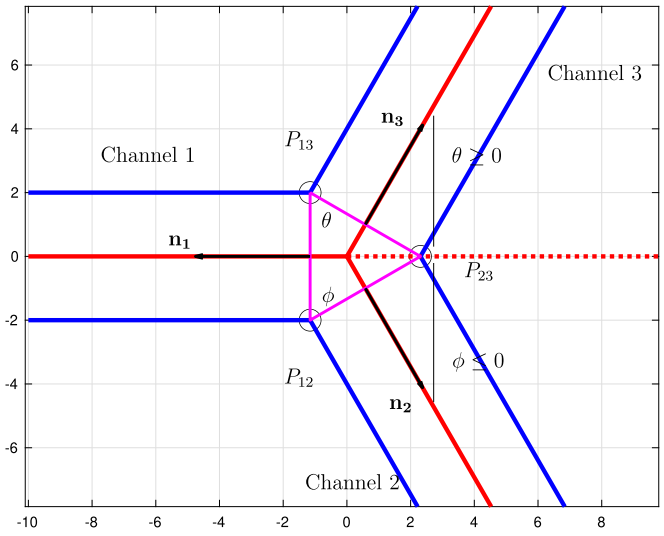

Fig. 4. A particular case: junction where the directions of the channels are perpendicular to the sides of the triangle. Parameters are $s_1 = s_2 = s_3 = 2$ and $\theta = -\phi = \frac{\pi}{3}$.

Therefore, conservation of mass and of the two components of momentum at the junction in this particular case yield

$$\begin{cases} -s_1 q_1 + s_2 q_2 + s_3 q_3 = 0, \\ \dfrac{q_1^2}{h_1} + \dfrac{1}{2} g h_1^2 = \dfrac{q_2^2}{h_2} + \dfrac{1}{2} g h_2^2 = \dfrac{q_3^2}{h_3} + \dfrac{1}{2} g h_3^2. \end{cases} \tag{29}$$

Note that in this case, the junction conditions do not depend on the angles with which the channels intersect. We thus recover the equal energy condition at the junction used by several authors, see [25] and references therein. This condition derives from the 2D momentum conservation at the junction, but we stress that it holds only for the particular case in which the channels are orthogonal to the sides of the triangle defining the junction.

Moreover, straightforward calculations show that equations (25) imply the geometry in Fig. 4. Since the conservation condition can be multiplied by a constant without changing the result, we see that for each pair of angles ϕ and θ there exists a one parameter set of sections $\lambda(s_1, s_2, s_3)$, with $\lambda > 0$ for which momentum conservation coincides with energy conservation.

Remark 3. The derivation leading to (29) proves that the present discussion is actually an *extension* of the junction conditions based on energy conservation. Only in the case of the particular combination of parameters satisfying (25), the junction Riemann solver does *not depend* on the angles between the channels. In particular, if all sections are equal, (25) implies that conservation of momentum coincides with conservation of energy only in the case $\theta = \frac{\pi}{3} = -\phi$ see Fig. 4.

We now consider the cases $\theta = \phi = 0$ and $\theta = -\phi = \pi/2$ which where excluded in the generic case described in section 3. We call:

- T-junction: $\theta = -\phi = \pi/2$.
- Straight channel: $\theta = \phi = 0$, $s_1 = s_2 + s_3$.

3.2.1. T-junction

In the case of a T-junction, for which the angles are equal to $\theta = -\phi = \pi/2$ and $s_2 = s_3$, the points P_{12}, P_{13} and P_{23} can be defined as in Fig. 5a, namely

$$P_{12}\begin{pmatrix} -s_2 \\ -s_1 \end{pmatrix}, P_{13}\begin{pmatrix} -s_2 \\ s_1 \end{pmatrix}, P_{23}\begin{pmatrix} s_2 \\ 0 \end{pmatrix}.$$

Equations (24) reduce to

$$\begin{cases} -s_1 h_1 v_1 + s_2 h_2 v_2 + s_2 h_3 v_3 = 0, \\ -2\left(h_1 v_1^2 + \dfrac{1}{2} g h_1^2\right) + \dfrac{1}{2} g h_2^2 + \dfrac{1}{2} g h_3^2 = 0, \\ -\left(h_2 v_2^2 + \dfrac{1}{2} g h_2^2\right) + h_3 v_3^2 + \dfrac{1}{2} g h_3^2 = 0. \end{cases}$$

When $s_2 \neq s_3$, the point P_{23} can be defined as in Fig. 5b, then

$$P_{12}\begin{pmatrix} -s_2 \\ -s_1 \end{pmatrix}, P_{13}\begin{pmatrix} -s_3 \\ s_1 \end{pmatrix}, P_{23}\begin{pmatrix} \min(s_2, s_3) \\ 0 \end{pmatrix}.$$

3.2.2. Straight channel

Now, we consider the case when $\theta = \phi = 0$ with $s_1 = s_2 + s_3$. There is a natural way to define points P_{12} and P_{13}, see Fig. 6. By symmetry, the y-coordinate of P_{23} should be set to 0 but the x-coordinate is undetermined. We fix $P_{23,x} = s_1$, thus

$$P_{12}\begin{pmatrix} 0 \\ -s_1 \end{pmatrix}, P_{13}\begin{pmatrix} 0 \\ s_1 \end{pmatrix}, P_{23}\begin{pmatrix} s_1 \\ 0 \end{pmatrix}$$

and equations (24) reduce to:

$$\begin{cases} -2h_1 v_1 + h_2 v_2 + h_3 v_3 = 0, \\ -2\left(h_1 v_1^2 + \dfrac{1}{2} g h_1^2\right) + \left(h_2 v_2^2 + \dfrac{1}{2} g h_2^2\right) + \left(h_3 v_3^2 + \dfrac{1}{2} g h_3^2\right) = 0, \\ -\dfrac{1}{2} g h_2^2 + \dfrac{1}{2} g h_3^2 = 0. \end{cases}$$

Note these conditions are independent of the sections and therefore we cannot extend our construction to the case of a single channel with a varying cross section with this configuration; see [29] or [2] for an exact solution of the Riemann problem for augmented shallow-water equations in the case of varying cross section.

4. Numerical scheme for shallow-water equations complemented with junction conditions

In this section, we couple a standard final volume scheme for the shallow water equations along each channel with the numerical flux consistent with our junction conditions (11)-(24).

4.1. One dimensional finite volume scheme

For the sake of simplicity, we will suppose that each channel has the same length, discretized with a uniform grid. Then, the computational domain in each channel is defined by the finite interval $[0, L]$, which is divided in M equal cells, of length $\Delta x = L/M$. The cell centers are given by $x_j = (j - \frac{1}{2})\Delta x$, $j = 1, \dots, M$. The numerical solution is piecewise constant and is defined as an approximation of the cell average of the exact solution U at time t in the j-cell given by

$$U_j(t) = \frac{1}{\Delta x} \int_{x_{j-\frac{1}{2}}}^{x_{j+\frac{1}{2}}} U(x,t)\, dx, \tag{30}$$

with appropriate boundary conditions for $U_0(\cdot)$ in channel 1 and $U_{M+1}(\cdot)$ on the two outgoing channels 2 and 3. The system is evolved until the final time T, with time step Δt. We denote by U_j^n the approximate value for the average of U in cell j at the discrete time $t_n = n\Delta t$. Hence, the finite volume approximation of system (2) can be written under the form

$$\frac{U_j^{n+1} - U_j^n}{\Delta t} = -\frac{1}{\Delta x}\left(\hat{F}^n_{j+\frac{1}{2}} - \hat{F}^n_{j-\frac{1}{2}}\right), \tag{31}$$

where

$$\hat{F}^n_{j-\frac{1}{2}} = F\left(U^n_{j-1}, U^n_j\right), \tag{32}$$

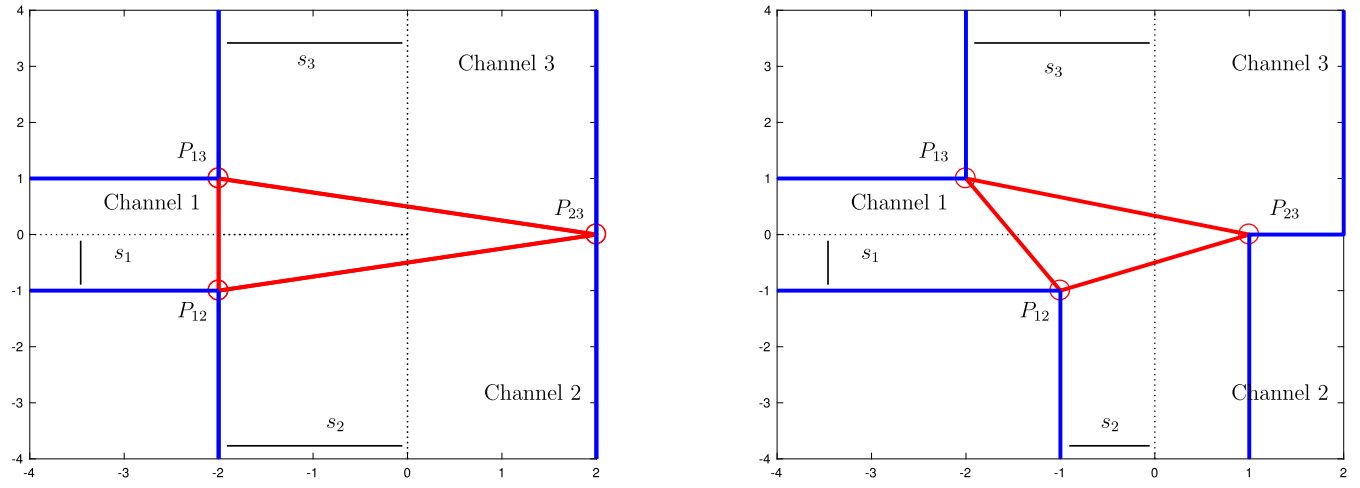

(a) Case when $s_2 = s_3$ (b) Case when $s_2 \neq s_3$

Fig. 5. Junction - Particular cases of the T-junction. Parameters are $\theta = -\phi = \frac{\pi}{2}$ and (a) $s_1 = 1$, $s_2 = s_3 = 2$ and (b) $s_1 = s_2 = 1$, $s_3 = 2$.

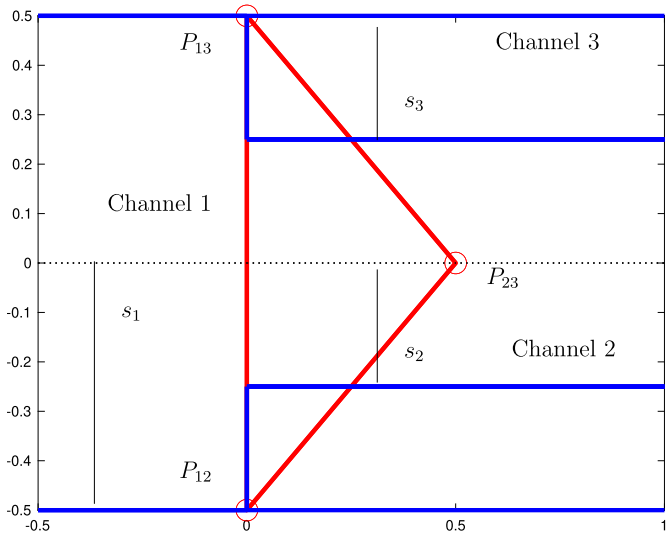

Fig. 6. Junction - Particular case of the straight channel. Parameters are $\theta = \phi = 0$ and $s_1 = 0.5$, $s_2 = s_3 = 0.25$.

with $F(\cdot,\cdot)$ a proper numerical flux. We apply a Godunov type numerical flux [31,34], computing the exact intermediate state for the Riemann problem between the two cells defined by $U_l = U^n_{j-1}$ and $U_r = U^n_j$ for $j = 1, \dots, M$.

From now on we shall add a channel index and we use the notation $U^n_{j,k}$, $j = 1, \dots, M$, to indicate the numerical solution along channel $k = 1, 2, 3$ computed at time t^n, in $x_{j,k}$. The time step Δt is fixed to satisfy the stability condition

$$\Delta t \leq \frac{\Delta x}{\max\limits_{k=1,2,3} \max\limits_{1 \leq j \leq M} \max \{|\lambda_1(U^n_{j,k})|, |\lambda_2(U^n_{j,k})|\}}, \tag{33}$$

where λ_1 and λ_2 are the eigenvalues defined in (6).

Finally, we use free-flow boundary conditions at the external boundaries, that is to say, we impose $U^n_{0,1} = U^n_{1,1}$, $U^n_{M+1,2} = U^n_{M,2}$ and $U^n_{M+1,3} = U^n_{M,3}$.

4.2. Junction conditions and coupling with the finite volume 1D scheme

Let us now explain how we insert the junction conditions (11)-(24) in the finite volume numerical scheme (31). Let us write scheme (31) in channel k, $k = 1, 2, 3$ under the following form:

$$\frac{U^{n+1}_{j,k} - U^n_{j,k}}{\Delta t} = -\frac{1}{\Delta x}\left(\hat{F}^n_{j+\frac{1}{2},k} - \hat{F}^n_{j-\frac{1}{2},k}\right). \tag{34}$$

In a channel network, the extreme point $x_{1,k}$ or $x_{M,k}$ can be either a *boundary point* or a *junction point* connected with other channels. In our setting $x_{M,1}$, $x_{1,2}$ and $x_{1,3}$ are junction points, while $x_{1,1}$, $x_{M,2}$ and $x_{M,3}$ are boundary points. At the external boundaries of the network, numerical tests use free-flow conditions, but other boundary conditions can naturally be used.

Let $U_k = (h_k, v_k)^T$, $k = 1, 2, 3$ be the solution to system (11)-(24) with $U^*_1 = U^n_{M,1}$, $U^*_2 = U^n_{1,2}$, $U^*_3 = U^n_{1,3}$ where $U^n_{M,1}$, $U^n_{1,2}$ and $U^n_{1,3}$ are the values computed by the 1D scheme along the channels. Then, at the junction points we impose $\hat{F}^n_{M+1/2,1} = f(U_1)$, $\hat{F}^n_{1/2,2} = f(U_2)$ and $\hat{F}^n_{1/2,3} = f(U_3)$.

4.3. Solving the non-linear system at the junction

Now, let us study the solutions to the nonlinear system at the junction. We recall the notation used in Sec. 3 and denote by h^*_k and v^*_k the approximate values of h and v near the junction at channel $k = 1, 2, 3$ given by the 1D numerical scheme, see also Sec. 4 for their exact definition. Let Ω be the open set of admissible states, $\Omega = \{h_k \in \mathbb{R}^+_*, v_k \in \mathbb{R}, |v_k| < \sqrt{g h_k}, k = 1, 2, 3\}$. The approximate values h_k and v_k are then obtained solving the non-linear system (24) with v_k given by (11). Let us denote

$$X = \begin{pmatrix} h_1 \\ h_2 \\ h_3 \\ v_1 \\ v_2 \\ v_3 \end{pmatrix}, \quad X^* = \begin{pmatrix} h^*_1 \\ h^*_2 \\ h^*_3 \\ v^*_1 \\ v^*_2 \\ v^*_3 \end{pmatrix} = \begin{pmatrix} h_{1,M} \\ h_{2,1} \\ h_{3,1} \\ v_{1,M} \\ v_{2,1} \\ v_{3,1} \end{pmatrix}.$$

We can rewrite the system under the following form

$$\Psi\left(X; X^*\right) = 0 \tag{35}$$

where $\Psi : \Omega \times \Omega \to \mathbb{R}^6$. In general, existence and uniqueness results for solutions to non linear systems are difficult to prove.

Assume that we have solved the system up to $t = t^n$, this gives the junction solution $X^{n,*}$ at the edges of the channels. Suppose that we have found a solution X^n such that $\Psi(X^n; X^{n,*}) = 0$. If we can prove that Det $D\Psi(X^n; X^{n,*}) \neq 0$, where $D\Psi$ denotes the Jacobian with respect to the first argument, then there exists a unique $X = X(X^*)$, for

$\|X^* - X^{n,*}\| < \epsilon$, with ϵ small enough, such that $\Psi(X; X^*) = 0$. Therefore, if the flow is smooth, one can find Δt small enough such that $\|X^{n+1,*} - X^{n,*}\| < \epsilon$ and the implicit function theorem guarantees that there exists a unique solution X^{n+1} such that $\Psi(X^{n+1}; X^{n+1,*}) = 0$. So, the procedure can be iterated provided one can prove at each step that $\text{Det } D\Psi(X^n; X^{n,*}) \neq 0$.

In the particular case when all waves are rarefactions, the relations (11) become

$$\begin{cases} v_1 + 2\sqrt{gh_1} = v_1^* + 2\sqrt{gh_1^*}, \\ v_2 - 2\sqrt{gh_2} = v_2^* - 2\sqrt{gh_2^*}, \\ v_3 - 2\sqrt{gh_3} = v_3^* - 2\sqrt{gh_3^*}, \end{cases} \tag{36}$$

and it is clear that the Jacobian $D\Psi$ does not depend on the data X^*. Thus, starting from a set of data X^* and a solution X such that $\Psi(X; X^*) = 0$, once one can prove that

$$\text{Det } D\Psi\left(X; X^*\right) \neq 0, \text{ for all } X^*, X \in \Omega \times \Omega, \tag{37}$$

the solution exists at each time step. Note that, for the steady solution $h = const.$ and $v = 0$ one has $X^* = (h, h, h, 0, 0, 0)^T$ and $\Psi(X; X^*) = 0$ for $X = X^*$, thus there exists at least one case for which $\Psi(X; X^*) = 0$.

Example 1. In the case when the channels are orthogonal to the sides of the triangle, we have

$$\Psi\left(X; X^*\right) = \begin{pmatrix} s_1 h_1 v_1 - s_2 h_2 v_2 - s_3 h_3 v_3 \\ h_1 v_1^2 + \frac{1}{2} g h_1^2 - h_2 v_2^2 - \frac{1}{2} g h_2^2 \\ h_1 v_1^2 + \frac{1}{2} g h_1^2 - h_3 v_3^2 - \frac{1}{2} g h_3^2 \\ v_1 + 2\sqrt{gh_1} - v_1^* - 2\sqrt{gh_1^*} \\ v_2 - 2\sqrt{gh_2} - v_2^* + 2\sqrt{gh_2^*} \\ v_3 - 2\sqrt{gh_3} - v_3^* + 2\sqrt{gh_3^*} \end{pmatrix}.$$

Simple algebra gives,

$$\begin{aligned} &\text{Det } D\Psi\left(X; X^*\right) \\ &= \text{Det} \begin{pmatrix} s_1(v_1 - \sqrt{gh_1}) & -s_2(v_2 + \sqrt{gh_2}) & -s_3(v_3 + \sqrt{gh_3}) \\ (v_1 - \sqrt{gh_1})^2 & -(v_2 + \sqrt{gh_2})^2 & 0 \\ (v_1 - \sqrt{gh_1})^2 & 0 & -(v_3 + \sqrt{gh_3})^2 \end{pmatrix} \\ &= \lambda_1(U_1)\lambda_2(U_2)\lambda_2(U_3) \\ &\quad \times \left(s_1 \lambda_2(U_2)\lambda_2(U_3) - s_2 \lambda_1(U_1)\lambda_2(U_3) - s_3 \lambda_1(U_1)\lambda_2(U_2)\right), \end{aligned}$$

where $\lambda_1(U_1), \lambda_2(U_2)$ and $\lambda_2(U_3)$ are defined at Eq. (6).

We can therefore conclude that since we are in the sub-critical case, for which $\lambda_1(U_1) < 0, \lambda_2(U_2) > 0, \lambda_2(U_3) > 0$, we have

$$\text{Det } D\Psi\left(X; X^*\right) < 0, \text{ for all } X^*, X \in \Omega,$$

which implies condition (37). This coincides with the case in which one assumes the continuity of the energy.

Example 2. *Case with vanishing velocities.*

Now, consider the case given by system (24)-(11), with only rarefaction waves. In order to simplify the expressions arising in the computations, we introduce the following notation

$$\begin{cases} \alpha_1 = \ell_1 \begin{pmatrix} 1 \\ 0 \end{pmatrix} \cdot \mathbf{n}_1 = -2s_1, \\ \alpha_2 = \ell_2 \begin{pmatrix} 1 \\ 0 \end{pmatrix} \cdot \mathbf{n}_2 = s_1 + \dfrac{s_2 \sin\theta + s_3 \sin\phi}{\sin(\theta - \phi)}, \\ \alpha_3 = \ell_3 \begin{pmatrix} 1 \\ 0 \end{pmatrix} \cdot \mathbf{n}_3 = s_1 - \dfrac{s_2 \sin\theta + s_3 \sin\phi}{\sin(\theta - \phi)}, \\ \beta_1 = \ell_1 \begin{pmatrix} 0 \\ 1 \end{pmatrix} \cdot \mathbf{n}_1 = \dfrac{s_1 \sin(\theta + \phi) - s_2 \sin\theta - s_3 \sin\phi}{\sin\phi \sin\theta}, \\ \beta_2 = \ell_2 \begin{pmatrix} 0 \\ 1 \end{pmatrix} \cdot \mathbf{n}_2 = -\dfrac{s_2 \cos\theta + s_3 \cos\phi}{\sin(\theta - \phi)} - \dfrac{s_1 \cos\phi - s_2}{\sin\phi}, \\ \beta_3 = \ell_3 \begin{pmatrix} 0 \\ 1 \end{pmatrix} \cdot \mathbf{n}_3 = \dfrac{s_2 \cos\theta + s_3 \cos\phi}{\sin(\theta - \phi)} - \dfrac{s_1 \cos\theta - s_3}{\sin\theta}, \\ \gamma_2 = \ell_2 \begin{pmatrix} \cos\phi \\ \sin\phi \end{pmatrix} \cdot \mathbf{n}_2 = \alpha_2 \cos\phi + \beta_2 \sin\phi, \\ \gamma_3 = \ell_3 \begin{pmatrix} \cos\theta \\ \sin\theta \end{pmatrix} \cdot \mathbf{n}_3 = \alpha_3 \cos\theta + \beta_3 \sin\theta, \end{cases}$$

such that

$$\Psi\left(X; X^*\right) = \begin{pmatrix} \alpha_1 h_1 v_1 + \gamma_2 h_2 v_2 + \gamma_3 h_3 v_3 \\ \alpha_1 \left(h_1 v_1^2 + \frac{1}{2} g h_1^2\right) + \left(\gamma_2 h_2 v_2^2 \cos\phi + \frac{\alpha_2}{2} g h_2^2\right) \\ \quad + \left(\gamma_3 h_3 v_3^2 \cos\theta + \frac{\alpha_3}{2} g h_3^2\right) \\ \frac{1}{2}\beta_1 g h_1^2 + \left(\gamma_2 h_2 v_2^2 \sin\phi + \frac{\beta_2}{2} g h_2^2\right) \\ \quad + \left(\gamma_3 h_3 v_3^2 \sin\theta + \frac{\beta_3}{2} g h_3^2\right) \\ v_1 + 2\sqrt{gh_1} - v_1^* - 2\sqrt{gh_1^*} \\ v_2 - 2\sqrt{gh_2} - v_2^* + 2\sqrt{gh_2^*} \\ v_3 - 2\sqrt{gh_3} - v_3^* + 2\sqrt{gh_3^*} \end{pmatrix}.$$

Since explicit computations are too difficult, we restrict ourselves to the particular case when solutions with vanishing velocities $v_1^n = v_2^n = v_3^n = 0$ at the junction exist, that is to say

$$X^n = \begin{pmatrix} h_1^n & h_2^n & h_3^n & 0 & 0 & 0 \end{pmatrix}^T.$$

We already note that $\mathbf{n}_1 + \mathbf{n}_2 + \mathbf{n}_3 = 0$, if $(h_1^*, h_2^*, h_3^*, v_1^*, v_2^*, v_3^*) = (h, h, h, 0, 0, 0)^T$, $X^n = (h_1, h_2, h_3, v_1, v_2, v_3)^T = (h, h, h, 0, 0, 0)^T$ is a trivial solution of system (24)-(11).

We prove that in this case $\text{Det } D\Psi(X; X^*) \neq 0$. In fact,

$$D\Psi\left(X; X^*\right) = \left(\begin{array}{ccc|ccc} 0 & 0 & 0 & \alpha_1 h_1 & \gamma_2 h_2 & \gamma_3 h_3 \\ \alpha_1 g h_1 & \alpha_2 g h_2 & \alpha_3 g h_3 & 0 & 0 & 0 \\ \beta_1 g h_1 & \beta_2 g h_2 & \beta_3 g h_3 & 0 & 0 & 0 \\ \hline \frac{\sqrt{g}}{\sqrt{h_1}} & 0 & 0 & 1 & 0 & 0 \\ 0 & -\frac{\sqrt{g}}{\sqrt{h_2}} & 0 & 0 & 1 & 0 \\ 0 & 0 & -\frac{\sqrt{g}}{\sqrt{h_3}} & 0 & 0 & 1 \end{array}\right)$$

and

$$\begin{aligned} &\text{Det } D\Psi\left(X; X^*\right) \\ &= g^{5/2} \text{Det} \begin{pmatrix} -\alpha_1\sqrt{h_1} & \gamma_2\sqrt{h_2} & \gamma_3\sqrt{h_3} \\ \alpha_1 h_1 & \alpha_2 h_2 & \alpha_3 h_3 \\ \beta_1 h_1 & \beta_2 h_2 & \beta_3 h_3 \end{pmatrix} \\ &= g^{5/2}\sqrt{h_1 h_2 h_3}\left(-\alpha_1(\alpha_2\beta_3 - \alpha_3\beta_2)\sqrt{h_2 h_3} - \gamma_2(\alpha_1\beta_3 - \alpha_3\beta_1)\sqrt{h_1 h_3}\right. \\ &\quad \left. + \gamma_3(\alpha_1\beta_2 - \alpha_2\beta_1)\sqrt{h_1 h_2}\right) \\ &= 2g^{5/2}\sqrt{h_1 h_2 h_3}(\sqrt{h_1 h_2}s_3 + \sqrt{h_1 h_3}s_2 + \sqrt{h_2 h_3}s_1) \times \left(\frac{4 s_2 s_3}{\sin(\theta - \phi)}\right. \\ &\quad \left. + \frac{(s_1 \sin(\theta - \phi) + s_3 \sin(\phi) - s_2 \sin(\theta))^2}{\sin(\theta - \phi)\sin(\phi)\sin(\theta)}\right) \end{aligned}$$

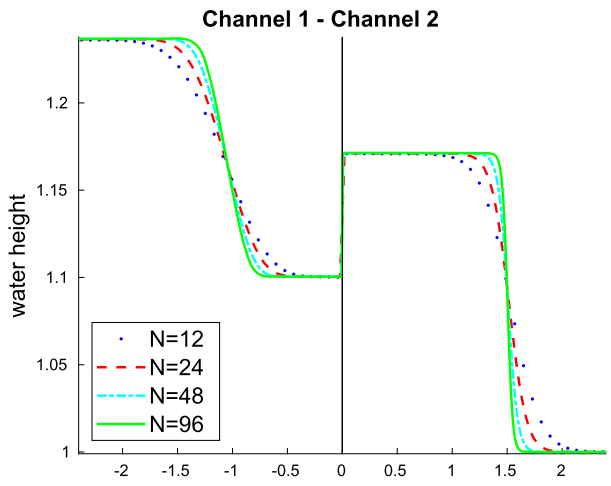

(a) height from channel 1 to 2 as a function of x

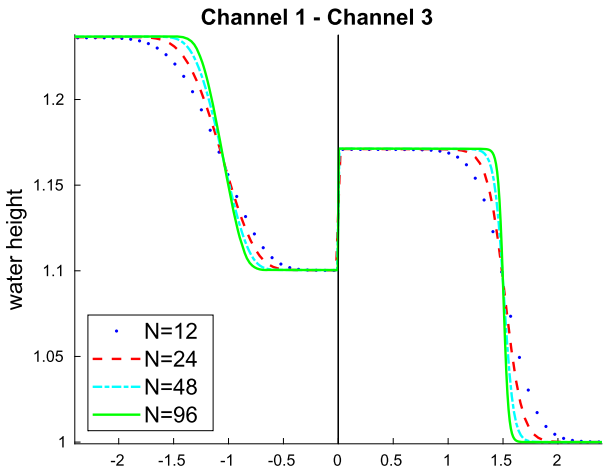

(b) height from channel 1 to 3 as a function of x

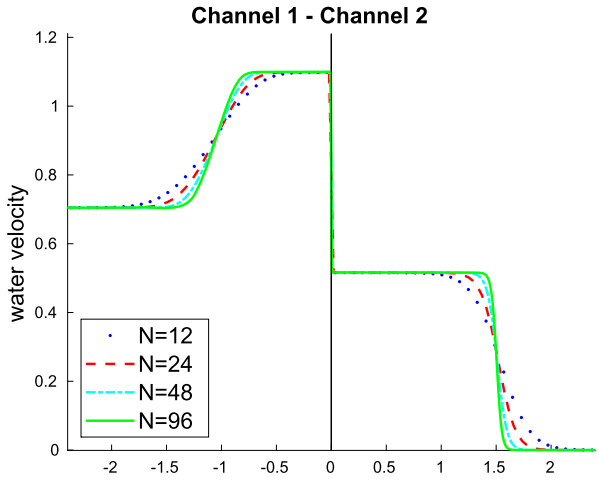

(c) velocity from channel 1 to 2 as a function of x

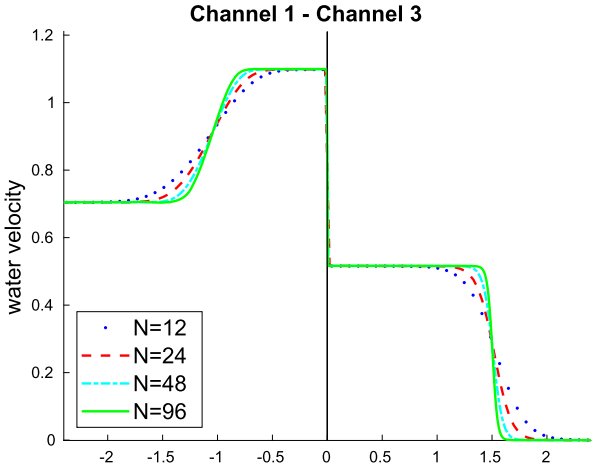

(d) velocity from channel 1 to 3 as a function of x

Fig. 7. Test 5.1: numerical convergence at time $T = 0.9$, after the shock has reached the junction; numbers of grid points are $N = 12, 24, 48, 96$. Initial data are given in (38).

We notice that this expression is the product of two terms: the first one, $2g^{5/2}\sqrt{h_1h_2h_3}(\sqrt{h_1h_2}s_3 + \sqrt{h_1h_3}s_2 + \sqrt{h_2h_3}s_1)$ is always positive since $h_1 > 0$, $h_2 > 0$, $h_3 > 0$.

The second term depends only on $s_1, s_2, s_3, \theta, \phi$, that is to say on the triangle geometry. This second term vanishes iff the triangle is degenerate, see Remark 1.

Therefore, excluding the case of a degenerate triangle,

$$\text{Det } D\Psi\left(X; X^*\right) \neq 0.$$

5. Numerical tests

In order to evaluate the effectiveness of our method we perform various tests consisting of a subcritical wave propagating across junctions of different geometries. For that purpose, we will use the numerical scheme presented in the previous section. First of all we check the numerical convergence of the scheme on the whole network under grid refinement. Then, we compare numerical simulations on a network with $\theta = \phi = 0$, with simulations on a single channel, to show the consistency of the junction conditions with the traditional one-dimensional Riemann solver. Subsequently, we increase θ and ϕ in order to enhance the influence of the angles in our junction conditions. We also investigate numerically the case when water flows out channels 1 and 3 and pours into channel 2. Finally, we compare the dynamics of the 1D solver with the numerical solution obtained with a two-dimensional code.

5.1. Convergence of the 1D numerical scheme

In this test case we check the numerical convergence of the 1D scheme (31) coupled with system (24)-(11) at the junction under grid refinement. We set the geometry parameters $s_1 = s_2 = s_3 = 1$, $\theta = -\phi = \pi/6$, $L_1 = L_2 = L_3 = 3.5$, where L_k is the length of channel k. The initial data in the three channels is

$$\begin{aligned} &v_k(x, t = 0) = 0, \quad k = 1, 2, 3, \ x \in [0, L_k], \\ &h_2(x, t = 0) = h_3(x, t = 0) = 1, h_1(x, t = 0) = \begin{cases} 1.5 & x \leq L_1/2 \\ 1 & x > L_1/2. \end{cases} \end{aligned} \tag{38}$$

We expect the formation of a rarefaction wave propagating backwards on channel 1 and a shock crossing the junction and traveling with positive speed along the two outgoing channels. In Fig. 7 we show the solution obtained after the water wave has reached the junction. The dynamic involves the three channels and we observe the convergence of the numerical solution under grid refinement. The number of grid points on each channel is $N = 12, 24, 48, 96$. We observe that the solution of system (24)-(11) at the junction does not depend

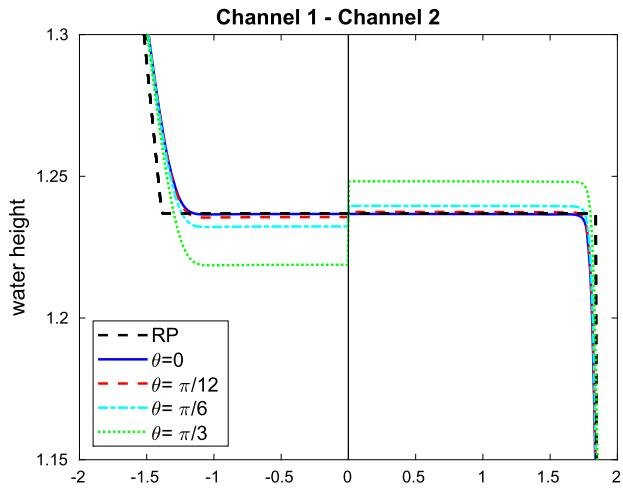

(a) height from channel 1 to 2 as a function of x

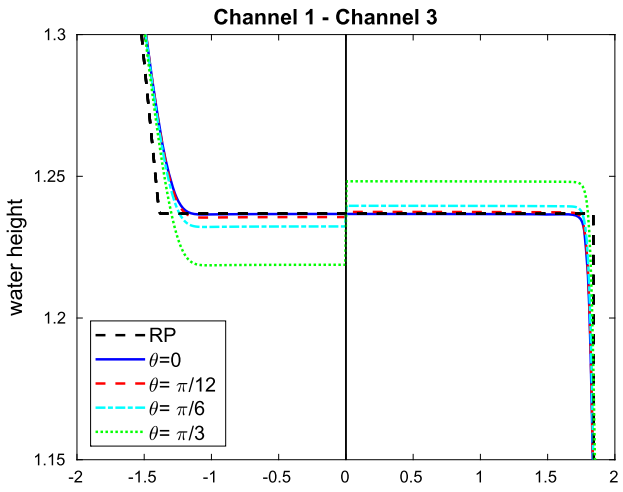

(b) height from channel 1 to 3 as a function of x

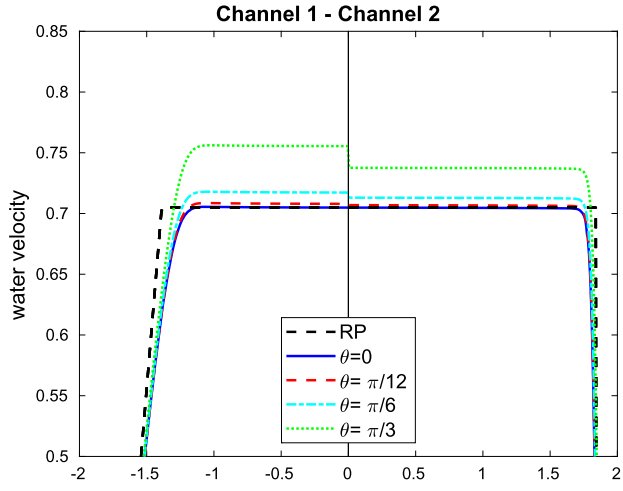

(c) velocity from channel 1 to 2 as a function of x

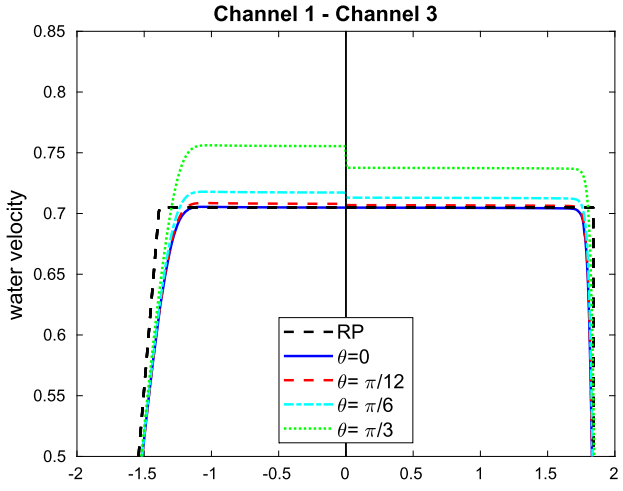

(d) velocity from channel 1 to 3 as a function of x

Fig. 8. Test 5.2: comparison of various symmetric geometries with the solution on a single channel at $T = 0.5$: $s_1 = 1$ and $s_2 = s_3 = 1/2$; $\phi = -\theta$ and $\theta = 0, \pi/12, \pi/6, \pi/3$. Black dashed line: 1D exact solution to shallow-water system on a single channel; Blue solid line: numerical solution for $\theta = \phi = 0$. Initial data are given in (38). The case $\theta = -\phi = \pi/3$ matches with the "1D energy" solution assuming equal energy at the junction, see (29).

on the grid parameter N, proving the consistency of the Riemann solver. We observe the formation of a stationary shock at the junction.

5.2. Comparison with the solution on a single channel

Here we study the influence of our junction conditions involving the angles θ and ϕ on the solution.

We set $s_1 = 1$ and $s_2 = s_3 = 1/2$, $L_1 = L_2 = L_3 = 5$ and the initial data are the same as in (38). In all tests we fix the grid parameters $\Delta x = 0.01$ on each channel and Δt to satisfy (33).

We first consider the case $\theta = \phi = 0$ and $s_1 = s_2 + s_3$ which corresponds to a single channel and for which an exact solution of the Riemann problem is known. As expected, the solution of our algorithm coincides with the exact solution computed on a single channel, i.e. without the junction, see the blue line and the black dashed line on Fig. 8.

Next, we change θ and ϕ to study the influence of the angles on the dynamics. Specifically, in Fig. 8 the angles vary symmetrically with $\theta = -\phi$ and $\theta = 0, \pi/12, \pi/6, \pi/3$. We observe that the symmetry of the configuration is preserved and that the solution varies monotonically increasing the angles and moving away from the single channel profile. Note that to see the dependence of the solution on the angles, it is essential to include an angle dependence in the junction condition. Notice that, the curve obtained for $\theta = -\phi = \pi/3$ is the solution assuming equal energy at the junction, see (29). From now on, this case will be called "1D energy".

In Fig. 9 we study the influence of a non symmetric variation of the angles: we fix $\theta = \pi/8$ and vary $\phi = -k\pi/8$ with $k = 0, 1, 2, 3$. We observe that the symmetry of the solutions of the two outgoing channels is lost and that water meets more resistance as channel 2 becomes more and more bent. So, the water level decreases in channel 2 and increases in channel 3. The solution on channel 1 does not change because the total lumen of the outgoing channels remains the same.

Finally, we compare the 1D solution fixing the two angles and varying the channel sizes. Specifically, we fix $\theta = -\phi = \pi/4$, $s_1 = s_2 = 1$ and consider $s_3 = 0.5, 1, 1.5, 2$. In Fig. 10 we observe that, as the section of channel 3 increases, the water height decreases in channels 1 and 3 and increases in channel 2. The water velocity in channels 2 and 3 follows the same behavior, while the velocity in channel 1 increases. However, the dynamics in channel 2 does not vary significantly.

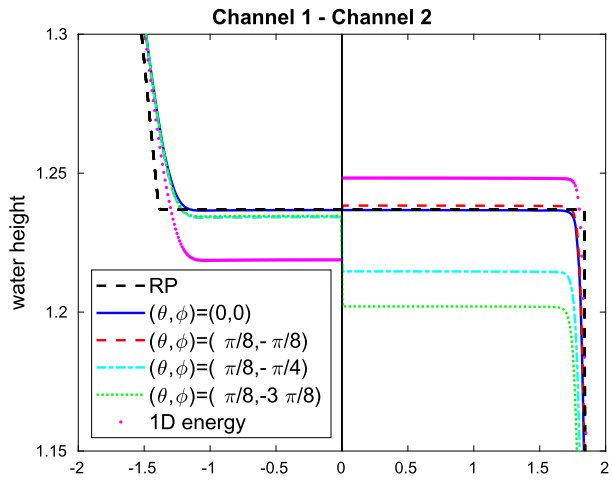

(a) height from channel 1 to 2 as a function of x

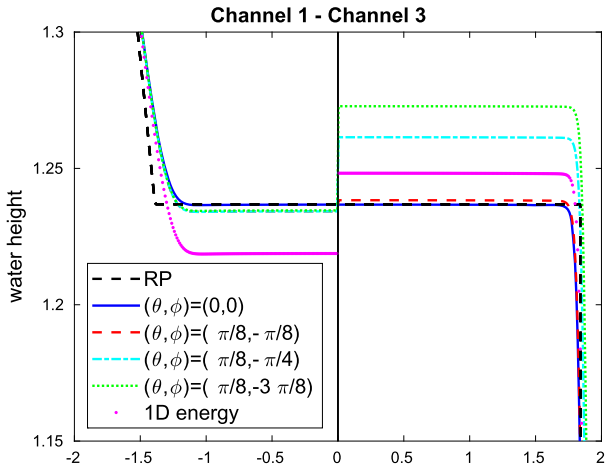

(b) height from channel 1 to 3 as a function of x

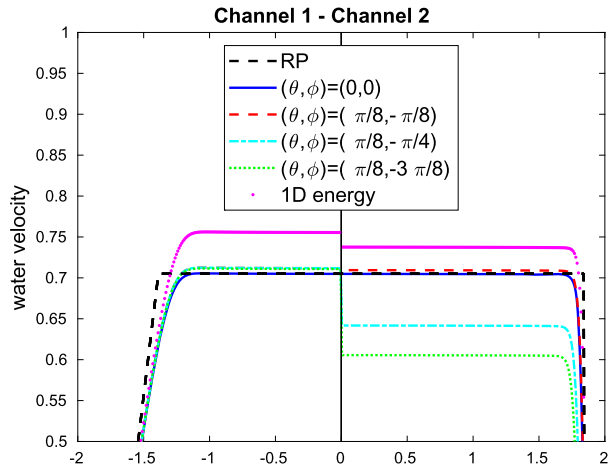

(c) velocity from channel 1 to 2 as a function of x

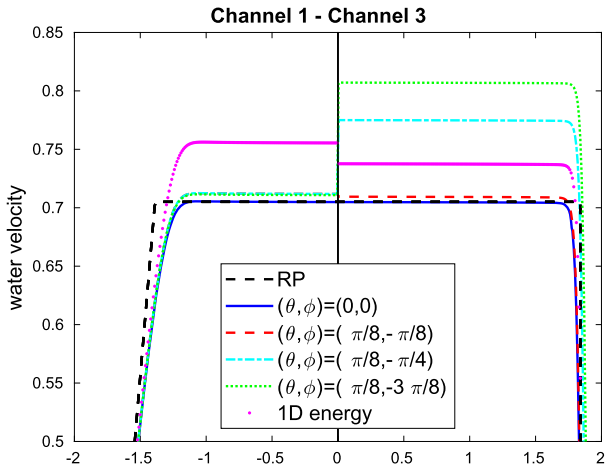

(d) velocity from channel 1 to 3 as a function of x

Fig. 9. Test 5.2: comparison of various triangle asymmetric geometries with different angles with the solution on a single channel at $T = 0.5$. $s_1 = 1$ and $s_2 = s_3 = 1/2$, $\theta = \pi/8$ fixed and $\phi = -\pi/8, -\pi/4, -3\pi/8$. Black dashed line: 1D exact shallow-water on a single channel; Blue solid line: numerical solution for $\theta = \phi = 0$. Initial data are given in (38). The curve "1D energy" is the solution assuming equal energy at the junction, see (29).

5.3. Merging channels

In this section we display numerical results for a 2-to-1 or *merging* junction for which the water flows from channels 1 and 3 towards channel 2. We set as initial data

$$v_k(x, t=0) = 0, \quad x \in [0, L_k], k = 1, 2, 3,$$
$$h_2(x, t=0) = 1, \; h_i(x, t=0) = \begin{cases} 1.5 & x \le L_i/2 \\ 1 & x > L_i/2. \end{cases}, \; i = 1, 3. \tag{39}$$

Then, we fix $s_1 = s_2 = s_3 = 1$, $\theta = \pi/3$. In Fig. 11, we compare the solutions obtained for $\phi = -\pi/3, -\pi/6, -\pi/12, 0$. As the angle ϕ widens, the water height increases in channel 1 and decreases in channel 3. This asymmetry explains why the dynamic in channel 2 is almost unaffected by the angle variation, the amount of water entering remains almost constant.

5.4. Comparison of 1D and 2D solutions

We compare our 1D solver with the 2D shallow water solution (12).

The numerical solution of (12) has been computed by the free and open source ToolBox *FullSWOF2D* (Full Shallow-Water equations for Overland Flow in 2D), which is a C++ code for simulations in two dimensions [11], which solves the shallow water equations with bottom topography on a rectangle R, and is able to deal with wet/dry fronts. We compute the solution on the rectangle in Fig. 12a with free flow boundary conditions $(v_x, v_y)^T \cdot \mathbf{n} = 0$ on the boundary of R. To obtain the 2D geometry of the junction we are interested in, we use a bottom topography which is $z_{in} = -1$ within the dashed region Ω and $z_{out} = 0$ in the complement Ω^C. We choose the initial water height so that $h + z_{in}$ is less than z_{out}. In this way, the water flows only inside the dashed region while Ω^C is seen as a dry state region. Thus the boundary conditions along the channel walls are naturally treated as wet/dry fronts occurring in R.

To compare the results of the 2D solution with the 1D code, the values of h, hv_x, hv_y of the 2D solution are sampled on the straight lines at the middle of the channels (black solid lines in Fig. 12b) of lengths L_k, $k = 1, 2, 3$. We compare the 1D velocity with the 2D velocity norm $\sqrt{v_x^2 + v_y^2}$. The mesh of the two-dimensional domain contains about 26×10^4 grid nodes.

We fix the channel lengths as $L_1 = L_2 = L_3 = 5$ and the simulation final time to $T = 1.5$. We set $s = s_1 = s_2 = s_3$, and we compare the 1D solution obtained with junction conditions (24)-(11) to the 2D solution with $s = 1,\ 0.5,\ 0.25$. As s decreases, the 2D configuration becomes closer to the 1D network. Recall that, in the 1D case, if $s = s_1 = s_2 = s_3$,

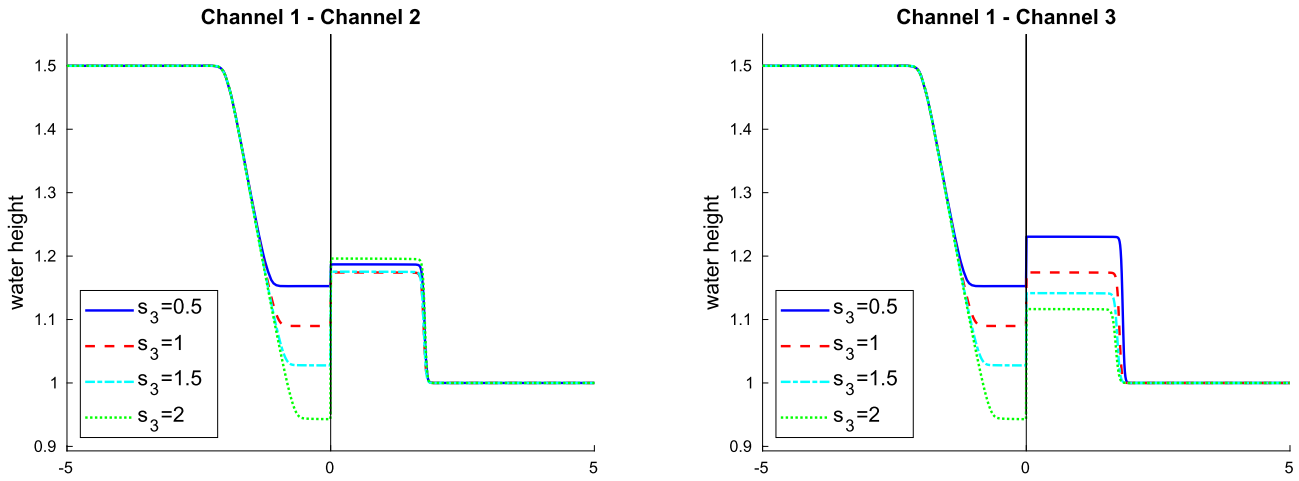

(a) height from channel 1 to 2 as a function of x

(b) height from channel 1 to 3 as a function of x

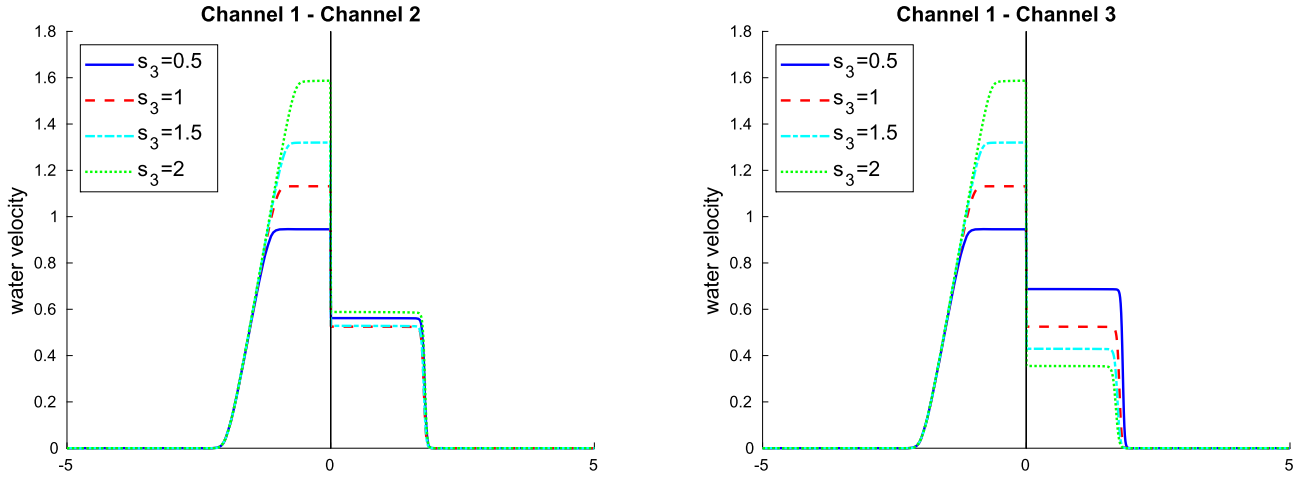

(c) velocity from channel 1 to 2 as a function of x

(d) velocity from channel 1 to 3 as a function of x

Fig. 10. Test 5.2: comparison of various geometries with different sections at $T = 0.5$. $\theta = -\phi = \pi/4$, $s_1 = s_2 = 1$ and $s_3 = 0.5, 1, 1.5, 2$. Initial data are given at Eq. (38).

the solution of the shallow water equations complemented with junction conditions (24)-(11) does not depend on the value of s.

We consider two different cases, a *diverging junction*, that it to say the case when water flows from the single channel 1 towards the two channels 2 and 3 and a *merging junction*, when the water flows from the two channels 1 and 3 towards the single channel 2. To fix a simple convention, we assume throughout the paper that the velocities $u_k > 0$, when the water is flowing from channel 1 to channels 2 and 3. However, this condition on the sign of the velocities is a mere convention. Thus, in the case of channels 1 and 3 pouring water in the junction, we will have $u_1 > 0, u_2 > 0, u_3 < 0$.

Diverging junction. We fix $\theta = \pi/3$, $\phi = -\pi/12$ and initial states as in (38) for the 1D configuration and for the 2D system such that

$$\begin{aligned} &v_{x,y}(x, y, t = 0) = 0 \quad (x, y) \in \Omega, \\ &h(x, y, t = 0) = \begin{cases} 1.5 & (x, y) \in \Omega \cap \{0 \le x \le L_1/2\} \\ 1 & \text{otherwise.} \end{cases} \end{aligned} \tag{40}$$

In Fig. 13, the 1D solution with junction conditions (24)-(11) is presented in solid red, the dotted black curve is the 1D solution assuming equal energy at the junction, as in [25]. We have three 2D solutions which are displayed in dashed blue, magenta and green for $s = 1,\ 0.5,\ 0.25$ respectively. Decreasing s we see that the 2D solutions converge towards the 1D wave front, both in the two shocks and the receding rarefaction. The only differences are observed in the flat intermediate states at the junction. The junction solver proposed in this work seems more accurate than the one with equal energy condition at the junction. Some wiggles appearing in the 2D solution might be due to numerical artefacts at the interface between dry and wet states of the 2D code. Therefore, the 1D solver developed in this article combines several advantages with respect to the 2D solver: it is easier to implement, the computation time is smaller, while ensuring good accuracy.

Merging junction. We fix $\theta = 5\pi/12$, $\phi = -3\pi/8$ and initial data as in (39) for the 1D configuration while for the 2D system as (40) with $h = 1.5$ in the right half of channel 3 too, see Fig. 12b.

As before, in Fig. 14, we superpose the 1D and 2D curves. Again, our 1D solution is displayed in solid red and the dotted black curve represents the solution with equal energy condition at the junction, [25]. The 2D solutions are drawn in dashed blue, magenta and green for $s = 1, 0.5, 0.25$ respectively. Decreasing s, we see that the 2D solutions converge towards the 1D water front, as expected.

T-junction. Here we consider a network with a T-configuration following [1]. We set $\phi = 0$ and $\theta = \pi/2$ and we assume asymmetric cross sections $s_1 = s_2 = 1$, $s_3 = 0.5$. The initial data are constant all along the three channels,

$$\begin{aligned} &v_k(x, t = 0) = 0, \\ &h_k(x, t = 0) = 0.05, \end{aligned} \qquad x \in [0, L_k], \quad k = 1, 2, 3. \tag{41}$$

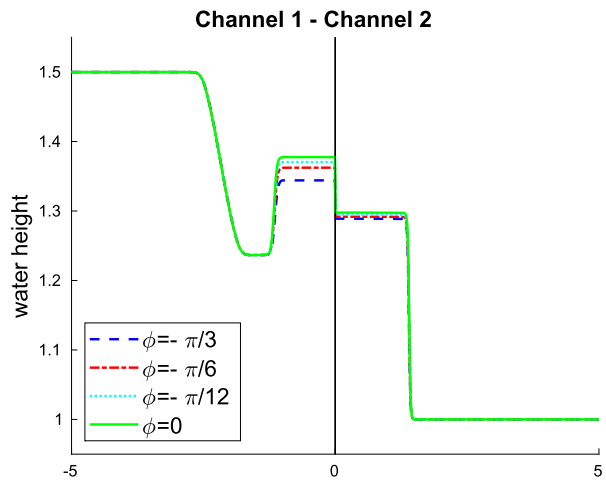

(a) height from channel 1 to 2 as a function of x

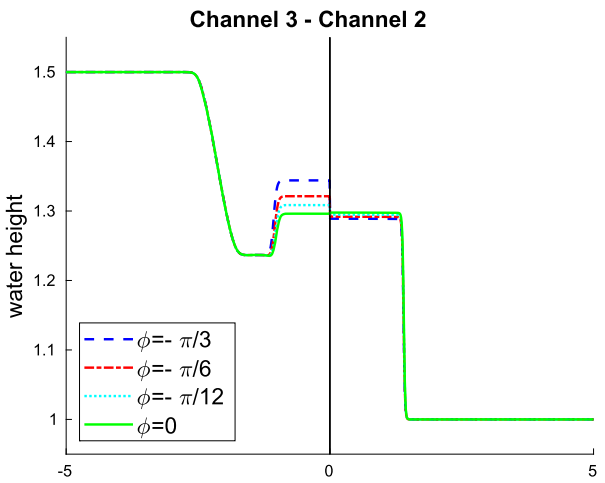

(b) height from channel 1 to 3 as a function of x

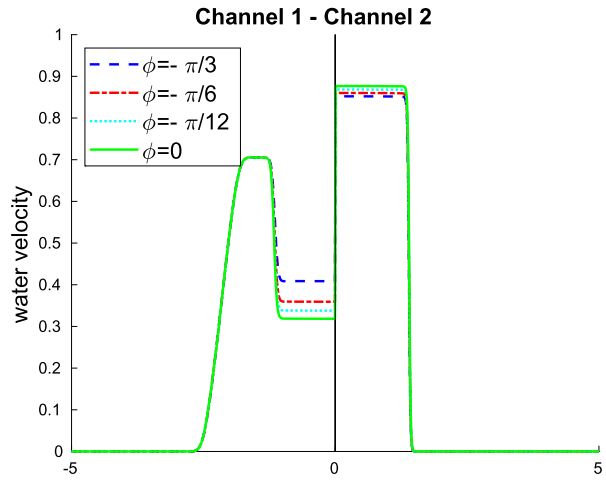

(c) velocity from channel 1 to 2 as a function of x

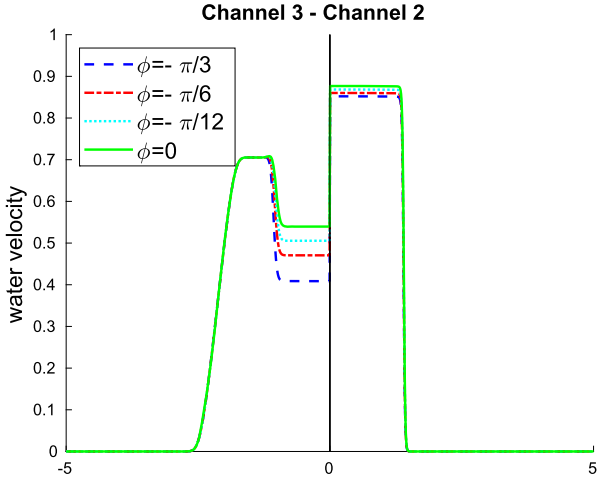

(d) velocity from channel 1 to 3 as a function of x

Fig. 11. Test 5.3: comparison of the solution for various geometries in the case of a merging at $T = 0.5$, $s_1 = s_2 = s_3 = 1$, $\theta = \pi/3$ and $\phi = -\pi/3, -\pi/6, -\pi/12, 0$. Initial data are given at Eq. (39). The curve $\theta = -\phi = \pi/3$ is the "1D energy" solution assuming equal energy at the junction, see (29).

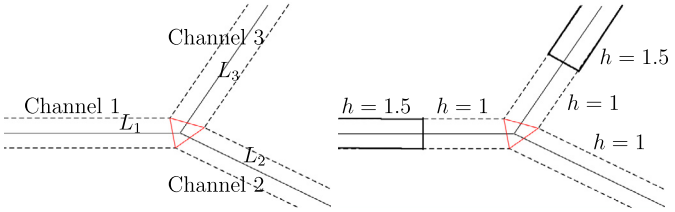

(a) 2D numerical domain for the comparison with the 1D geometry

(b) 2D initial water height in a merging junction

Fig. 12. 2D numerical geometry.

The velocity at the inflow of channel 1, is given by the relation

$$v_1(t) = 0.4 \exp(-0.5(t-3)^2). \tag{42}$$

We compare the solution obtained by our method and the solution obtained by the "1D energy" solver with the solution yielded by our 2D solver. Results are shown in Fig. 15. The obtained solutions can be compared with the results in [1] (Figs. 10–11). The two curves given by the 1D methods follow the main course of the 1D solution shown in [1]. They differ in their estimation of the water height from channel 1 to the other two channels. Our angle-dependent algorithm (in blue) captures the solution better on channels 1 and 3, which is influenced by the network configuration since it is at 90 degrees with respect to the direction of the water flow; on the other hand, our procedure seems to overestimate the water height in channel 2 (the horizontal extension of the first channel). The "1D energy" approach (in red) has the opposite behavior. It gives a better estimate on channel 2, which is along the direction of the incoming water flow, and overestimates the solution on channel 3. The estimate of the speed of the shock wave propagating along the two outgoing channels given by the two approaches is similar.

6. Conclusions

In this paper we have constructed a model for shallow water equations on networks by deriving junction conditions that depend on the angles of the geometry. We have also presented a numerical solver for one dimensional channels in a network. The solver is based on a finite volume scheme in each channel and coupling conditions at the junction are obtained with a single 2D element at the junction across which mass and the two components of momentum are conserved. This approach allows to take into account quite general geometries including the dependence on the angles with which the channels intersect at the junction and the sections of the channels.

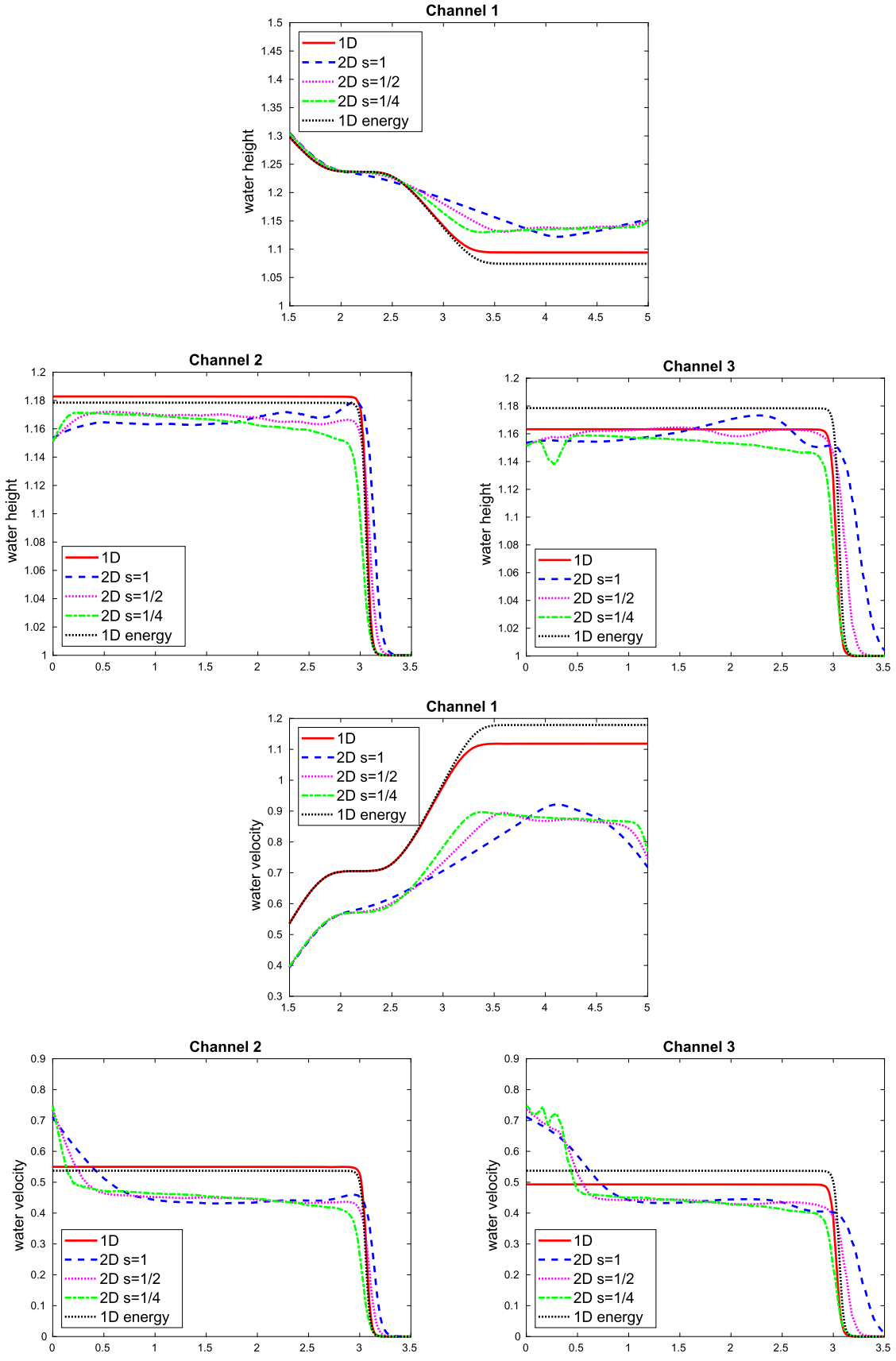

Fig. 13. Test 5.4, *diverging junction*: comparison of 2D with 1D solutions at $T = 1.5$: $\theta = \frac{\pi}{3}$ and $\phi = -\frac{\pi}{12}$, $L_1 = L_2 = L_3 = 5$, $s_1 = s_2 = s_3 = s$ with $s = 1,\ 0.5,\ 0.25$ (in the 2D case). The 1D solution with junction conditions (24)-(11) is displayed in solid red, the 1D solution with equal energy condition in dotted black, the 2D solution with $s = 1,\ 0.5,\ 0.25$ in dashed blue, magenta and green. Initial data are given at Eq. (38) (1D case) and Eq. (40) (2D case).

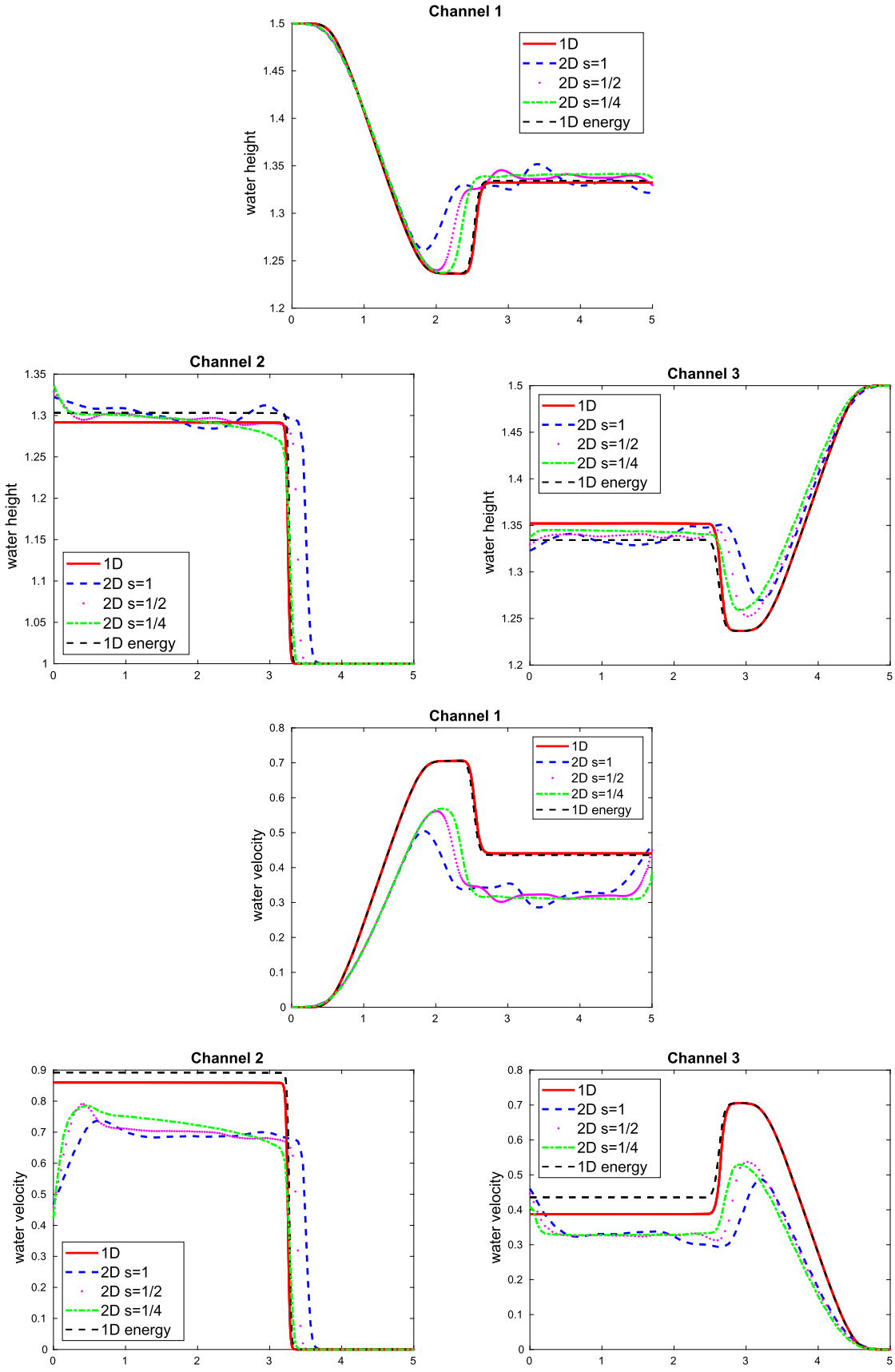

Fig. 14. Test 5.4, *merging junction*: comparison of 2D with 1D solutions at $T = 1.5$: $\theta = 5\pi/12$, $\phi = -3\pi/8$, $L_1 = L_2 = L_3 = 5$, $s_1 = s_2 = s_3 = s$ with $s = 1,\ 0.5,\ 0.25$ (in the 2D case). The 1D solution with junction conditions (24)-(11) is displayed in red, the 1D solution with equal energy condition in dotted black, the 2D solution with $s = 1,\ 0.5,\ 0.25$ in dashed blue, solid magenta and solid green. Initial data are given at Eq. (39) (1D case) and Eq. (40) with $h = 1.5$ in the right half of channel 3 (2D case).

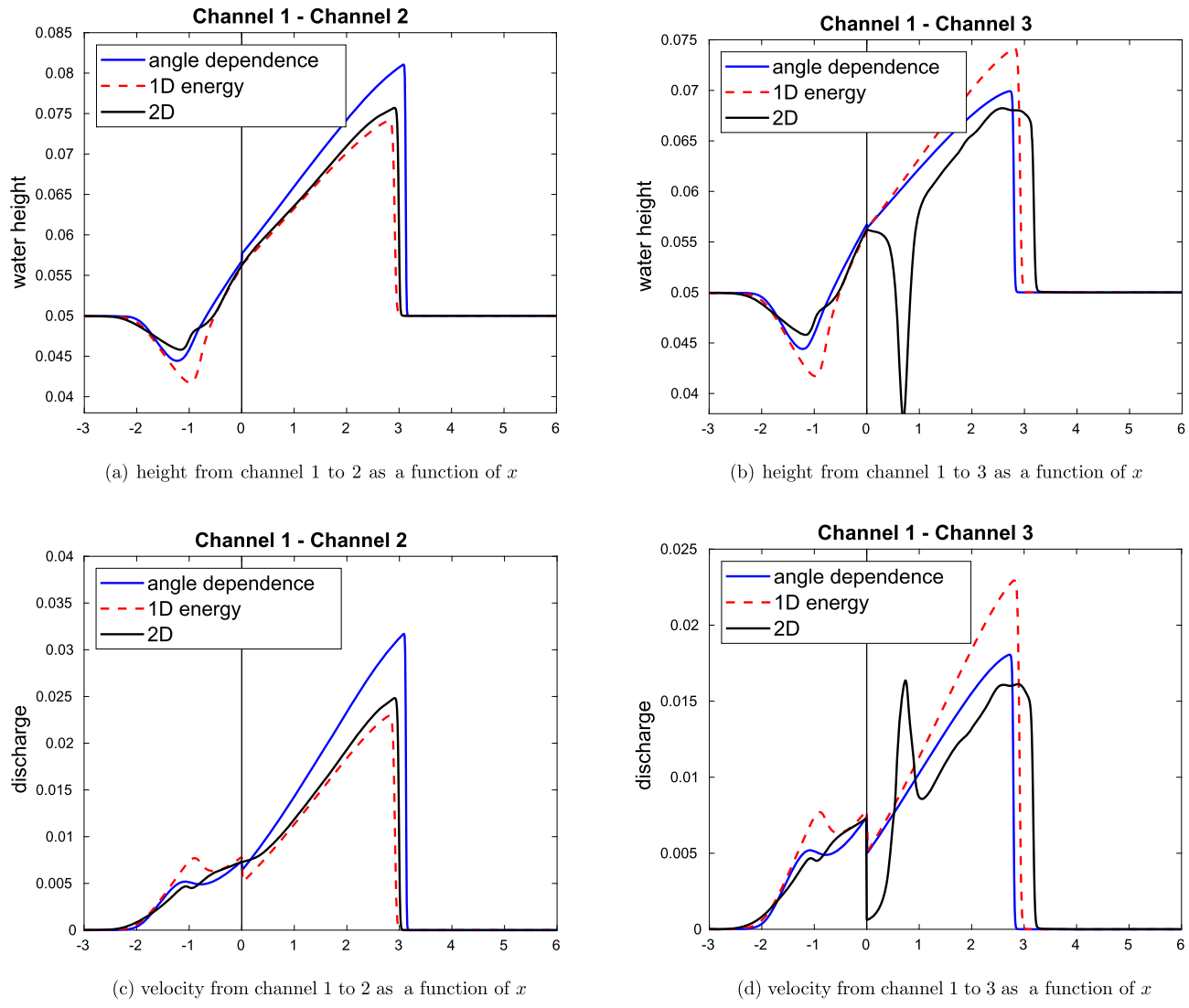

(a) height from channel 1 to 2 as a function of x

(b) height from channel 1 to 3 as a function of x

(c) velocity from channel 1 to 2 as a function of x

(d) velocity from channel 1 to 3 as a function of x

Fig. 15. Test: solution at $T = 8$. $\theta = \pi/2$, $\phi = 0$, $s_1 = s_2 = 1$ and $s_3 = 0.5$. Initial data are given at Eq. (41) and inflow velocity at Eq. (42).

The solver is based on the assumption that the flow across the junction is fluvial. Future work on this topic will be concentrated on the case of torrential flows and on the dependence of the bottom topography.

The extension of the proposed procedure to the more general case of a junction formed by $N > 3$ channels is left to future work. It could be handled in several ways. One possibility could be using more than one triangle within the junction, i.e. for the case $N = 4$, one could consider two three-channel junctions, each represented by a triangle, which faces the two channels on two sides, and the second triangle on the third side. This would mean to apply our construction twice, in a sort of cascade. A second possibility would be to consider a single 2D element, internal to the junction, with a shape suited to the geometry of the junction (for instance, a quadrilateral element for the case $N = 4$), leading to an under-determined system to be solved with a least square method.

Acknowledgements

This work was partly supported by MIUR (Ministry of University and Research) PRIN2017 project number 2017KKJP4X.

References

[1] Francesca Bellamoli, Lucas O. Müller, Eleuterio F. Toro, A numerical method for junctions in networks of shallow-water channels, Appl. Math. Comput. 337 (2018) 190–213.

[2] R. Bernetti, V.A. Titarev, E.F. Toro, Exact solution of the Riemann problem for the shallow water equations with discontinuous bottom geometry, J. Comput. Phys. 227 (6) (2008) 3212–3243.

[3] Edoardo Bocchi, Jiao He, Gastón Vergara-Hermosilla, Modelling and Simulation of a Wave Energy Converter, 2019.

[4] Raul Borsche, Numerical schemes for networks of hyperbolic conservation laws, Appl. Numer. Math. 108 (2016) 157–170.

[5] Alberto Bressan, Suncica Canic, Mauro Garavello, Michael Herty, Benedetto Piccoli, Flows on networks: recent results and perspectives, EMS Surv. Math. Sci. 1 (1) (2014) 47–111.

[6] Maya Briani, Benedetto Piccoli, Fluvial to torrential phase transition in open canals, Netw. Heterog. Media 13 (4) (2018) 663–690.

[7] Maya Briani, Benedetto Piccoli, Jing-Mei Qiu, Notes on RKDG methods for shallow-water equations in canal networks, J. Sci. Comput. 68 (3) (Sep. 2016) 1101–1123.

[8] Jean-Guy Caputo, Denys Dutykh, Bernard Gleyse, Coupling conditions for water waves at forks, Symmetry 11 (3) (2019) 434.

[9] Rinaldo M. Colombo, Michael Herty, Veronika Sachers, On 2 × 2 conservation laws at a junction, SIAM J. Math. Anal. 40 (2) (2008) 605–622.

[10] Adhémar Jean-Claude de Saint-Venant, et al., Théorie du mouvement non-permanent des eaux, avec application aux crues des rivières et à l'introduction des marées dans leur lit, C. R. Acad. Sci. Paris 73 (147–154) (1871) 5.

[11] Olivier Delestre, Frédéric Darboux, Francois James, Carine Lucas, Christian Laguerre, Stéphane Cordier, Fullswof: full shallow-water equations for overland flow, J. Open Sour. Softw. 2 (20) (2017) 448.

[12] A.I. Delis, Th. Katsaounis, Numerical solution of the two-dimensional shallow water equations by the application of relaxation methods, Appl. Math. Model. 29 (8) (2005) 754–783.

[13] C. Escalante, M.J. Castro, M. Semplice, Very high order well-balanced schemes for non-prismatic one-dimensional channels with arbitrary shape, Appl. Math. Comput. 398 (2021).
[14] Mauro Garavello, A review of conservation laws on networks, Netw. Heterog. Media 5 (3) (2010) 565.
[15] Mauro Garavello, Benedetto Piccoli, Riemann solvers for conservation laws at a node, in: Hyperbolic Problems: Theory, Numerics and Applications, in: Proc. Sympos. Appl. Math., vol. 67, Amer. Math. Soc., Providence, RI, 2009, pp. 595–604.
[16] J.-F. Gerbeau, B. Perthame, Derivation of viscous Saint-Venant system for laminar shallow water; numerical validation, Discrete Contin. Dyn. Syst., Ser. B 1 (1) (2001) 89–102.
[17] Rabih Ghostine, Georges Kesserwani, Robert Mose, José Vazquez, Abdellah Ghenaim, Caroline Gregoire, A confrontation of 1D and 2D RKDG numerical simulation of transitional flow at open-channel junction, Int. J. Numer. Methods Fluids 61 (7) (2009) 752–767.
[18] Rabih Ghostine, Jose Vazquez, Abdelali Terfous, Robert Mose, Abdellah Ghenaim, Comparative study of 1D and 2D flow simulations at open-channel junctions, J. Hydraul. Res. 50 (2) (2012) 164–170.
[19] Rabih Ghostine, Jose Vazquez, Abdelali Terfous, N. Rivière, Abdellah Ghenaim, Robert Mosé, A comparative study of 1D and 2D approaches for simulating flows at right angled dividing junctions, Appl. Math. Comput. 219 (10) (2013) 5070–5082.
[20] Mouhamadou Samsidy Goudiaby, Guinilla Kreiss, A Riemann problem at a junction of open canals, J. Hyperbolic Differ. Equ. 10 (03) (2013) 431–460.
[21] Martin Gugat, Optimal nodal control of networked hyperbolic systems: evaluation of derivatives, Adv. Model. Optim. 7 (1) (2005) 9–37.
[22] Martin Gugat, Guenter Leugering, Global boundary controllability of the Saint-Venant system for sloped canals with friction, Ann. Inst. Henri Poincaré, Anal. Non Linéaire 26 (1) (2009) 257–270.
[23] Martin Gugat, Guenter Leugering, E.J.P. Georg Schmidt, Global controllability between steady supercritical flows in channel networks, Math. Methods Appl. Sci. 27 (7) (2004) 781–802.
[24] Michael Herty, Nouh Izem, Mohammed Seaïd, Fast and accurate simulations of shallow water equations in large networks, Comput. Math. Appl. 78 (6) (2019) 2107–2126.
[25] Michael Herty, Mohammed Seaïd, Assessment of coupling conditions in water way intersections, Int. J. Numer. Methods Fluids 71 (11) (2013) 1438–1460.
[26] Helge Holden, Nils Henrik Risebro, Riemann problems with a kink, SIAM J. Math. Anal. 30 (3) (1999) 497–515.
[27] P.M. Jacovkis, One-dimensional hydrodynamic flow in complex networks and some generalizations, SIAM J. Appl. Math. 51 (04) (1991) 948–966.
[28] Georges Kesserwani, Rabih Ghostine, José Vazquez, Robert Mosé, Maher Abdallah, Abdellah Ghenaim, Simulation of subcritical flow at open-channel junction, Adv. Water Resour. 31 (2) (2008) 287–297.
[29] Philippe G. Lefloch, Mai Duc Thanh, The Riemann problem for fluid flows in a nozzle with discontinuous cross-section, Commun. Math. Sci. 1 (4) (2003) 763–797.
[30] Guenter Leugering, JP Georg Schmidt, On the modelling and stabilization of flows in networks of open canals, SIAM J. Control Optim. 41 (1) (2002) 164–180.
[31] Randall J. LeVeque, et al., Finite Volume Methods for Hyperbolic Problems, vol. 31, Cambridge University Press, 2002.
[32] Alessia Marigo, Entropic solutions for irrigation networks, SIAM J. Appl. Math. 70 (5) (2010) 1711–1735.
[33] Arne Roggensack, A kinetic scheme for the one-dimensional open channel flow equations with applications on networks, Calcolo 50 (4) (2013) 255–282.
[34] Eleuterio F. Toro, Riemann Solvers and Numerical Methods for Fluid Dynamics: A Practical Introduction, Springer Science & Business Media, 2013.